A quantitative analysis of multi-scale response of CMP pad: quasi-static and dynamic characterization of dry and wet pad

by

Sunil Doddabasanagouda

A thesis submitted to the graduate faculty

in partial fulfillment of the requirements for the degree of

MASTER OF SCIENCE

Major: Mechanical Engineering

Program of Study Committee:
Abhijit Chandra, Co-major Professor
Ashraf Bastawros, Co-major Professor
Thomas J. Rudolphi
Palaniappa A. Molian

Iowa State University

Ames, Iowa

2004

Graduate College
Iowa State University

This is to certify that the master's thesis of

Sunil Doddabasanagouda

has met the thesis requirements of Iowa State University

Signatures have been redacted for privacy

TABLE OF CONTENTS

LIST OF FIGURES

ABSTRACT

The characteristics of pad deformation and its surface morphology control the quality and efficacy of chemical mechanical planarization (CMP) process. The salient structural features of the pad (cell size, cell wall thickness & surface roughness) constitute structures that have several small length scales. The effect of these various length scales (micro & nano) on the mechanical response of the pad under different condition remains largely unexplored due to the deficiency of appropriate experimental techniques to characterize local deformation. To reveal the intricacy involved in the deformation of the CMP pad, an experimental and theoretical approach has been devised. The dry and wet IC-1000 pad responses are examined at different length scales using a nano-indenter with a conical tip of $1\mu m$ radius and a flat-punch of $30\mu m$ radius. The wet pad measurements showed degradation of the pad stiffness, which is attributed to water absorption within a micron of pad cell membrane. This reduction of stiffness is not significant because the pad material is impermeable to water and most of the water penetrates only the topmost layer of voids in the material. The load-indentation depth plots showed different characteristic trends with varying stiffness at different loading ranges. The measurements showed the competition between the local indentation, cell membrane bending and the bulk response of the porous pad. These different deformation mechanisms are utilized to construct an analytical model for effective pad stiffness. The model prediction matches well with the force-indentation depth measurements. An experimental measurement of the linear viscoelastic behavior of the surface of the pad in contact with a conical indenter is obtained. Variation of stiffness, damping coefficient, relaxation time with frequency and depth is obtained using a simple mechanical Voigt model in the Dynamic Model for Nanoindenter system, which is in contact with specimen. Such physically based model can be utilized to optimize the pad microstructure and morphology to control the applied force partitioning and the characteristics of the material removal rates.

CHAPTER 1. INTRODUCTION

With the advent of shallow trench isolation (STI) and copper interconnects, chemical mechanical polishing (CMP) has emerged as one of the most important operation in the fabrication of integrated circuits. CMP is a process for surface planarization, aided by the combined actions of the chemical etching and mechanical polishing. It provides the needed local die planarization and global wafer surface uniformity. The planarization process in CMP involves complex interactions between the wafer, polishing pad, chemical slurry and abrasive particles present in the slurry.

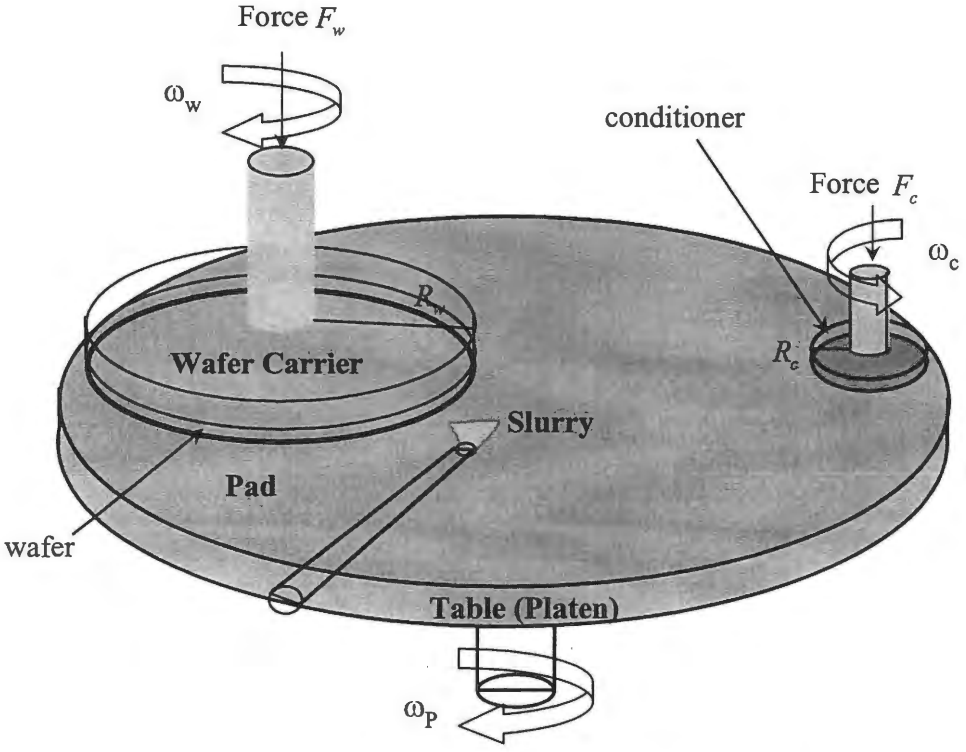

Figure 1.1 Schematic representation of CMP setup

In a CMP process material removal is accomplished by pressing a wafer into a relatively soft pad flooded with abrasive slurry while both the pad and the wafer are rotated as shown in Fig 1.1. The wafer rests on a backing plate, which is rotating about its own axis. The wafer is then pressed down against the pad, which is attached to a rotating platen disk [Steigerwald

1997]. A conditioner (diamond abrasive disc or wheel) is used to refresh the polishing pad surface. Generally, the conditioning disc is mounted on a powered rotating chuck that can be lowered on to the pad surface (Fig 1.1). During CMP, abrasive slurry with various process specific chemical compounds is used to soften the surface of the wafer [Hsu 2002] and the particle sizes in typical slurry are on the order of a few tens of nanometers. The chemical composition and pH of the slurry are important and depend on the material being polished. For planarizing an oxide layer, a high pH alkali-based solution is often used, while a low pH; oxidizer-based solution is commonly used for metals. In general the chemical reaction at the wafer surface makes the surface material susceptible to mechanical abrasion by the abrasive in the slurry. For metal removal, thee solution oxidizes the surface and the product reacts with the acid to form salt which is then polished in a similar fashion to the oxide removal [Nguyen et al 2000]. Removal rate stability (wafer to wafer variation), nonuniformity (both wafer-scale and die-scale) control and cost of ownership are some of the important issues in CMP application in IC manufacturing. Slurry, pad and carrier are the three major components with different functions in a CMP system setup. Understanding their function is the first step in the modeling and simulation of CMP processes. The main objective of this research is to investigate into the materials and mechanics aspect of CMP pad.

The mechanical properties, which are generally believed to influence pad performance, are: Young's modulus, Poisson's ratio, hardness, compressibility, viscoelastic properties, surface roughness and liquid permeability. In the material removal process, the pad must hold abrasives and transfer the load to the abrasive. Izumitani (1979) found that to satisfy these requirements, the pad must be viscoelastic so that the polishing grain can be embedded and at the same time, be rigid enough to transmit the load. In other words, the pad should have viscoelastic characteristics and is generally made of polymeric materials such as polyurethane for CMP pads. The viscoelastic deformation of the pad also plays an important role in the planarization process.

The applied pressure by the pad on the wafer surface depends on the topography of the wafer surface. Because of the flexibility of the pads, the resulting profiles depend on both the stiffness of the pad as well as the density and spacing of elevated features on the wafer surface. To satisfy the different requirements for CMP, different kinds of pads have been

developed. Some are for bulk polishing where removal rate is the major concern; others are for final finish where surface finish and defect reduction are major concerns. Pads are classified into four kinds according to their structural characteristics:

- Microporous synthetic leathers

Its structure is high porosity film on substrate and its microstructure is complex foam with vertically oriented channels. It is mainly used for Si final polish, metal damascene CMP and post-CMP buff.

- Felts and polymer impregnated felts (e.g., Suba IV)

Its structure is felted fiber with polymer binder and its microstructure is continuous channels between fibers. It is mainly used for Si stock polish and W damascene CMP.

- Unfilled textured polymer films

Its structure is a solid polymer sheet with surface texture and it is mainly used for ILD CMP, Shallow Trench Isolation (STI) and metal dual damascene.

- Filled polymer films (e.g., IC 1000 and IC 1400)

Its structure is solid urethane sheet with filler such as voids, SiO_2, CeO_2 etc and its microstructure is a closed cell and open cell foam. It is mainly used for ILD CMP and metal damascene. Fig. 1.2 shows a SEM picture of IC 1000 pad and it is closed cell polyurethane foam with voids that average about $50\mu m$ in diameter [Borucki 2002].

Pad manufacturing processes (e.g., felting, casting, laminating) will decide its microstructure. The micro or macro structures of pad will influence the polishing result. During CMP, pad surface is also planarized. Pad asperities are flattened by the abrasion of slurry particles and wafer surface. The abraded pad material, abrasive particles and re-deposited wafer surface material fill the pad pores, causing glaze [Bajaj et al 1994]. This result in obstruction of slurry transportation and the removed material cannot be moved out of the system. Also, pad deformation due to its viscoelastic properties leads to a bowl-shaped trench into the pad surface. In order to obtain consistent and reproducible polishing results it is important to have the pad treated at regular intervals. To stabilize pad surface, pad conditioning is used to bring the pad back to flat and remove materials from the pores.

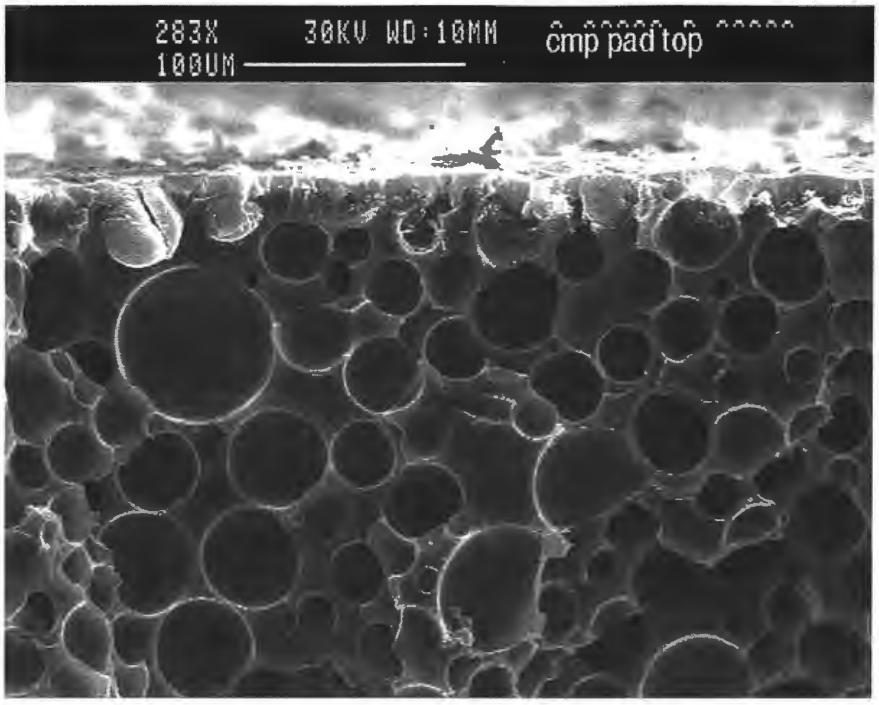

Figure 1.2 SEM picture of IC 1000 pad [Borucki 2002]

In a CMP process a relationship between pad properties and polishing performance is important and complex because: many aspects of polishing depend on scale-level, many pad properties are strongly interdependent, polishing pad have composite structures and polishing is a wet dynamic process.

Effects of pad properties on polishing performance are:

- Planarity / dishing-erosion
  - Pad hardness; modulus; stiffness
- Defectivity
  - Pad hardness; capability to remove polishing residue
- Removal rate
  - Slurry transport; slurry retention capability
- Non-Uniformity
  - Slurry transport; pad hardness; compressibility
- Pad life

- Conditioning method, thermal stability

Development of future pad materials will require an increased understanding of how the pad affects the CMP process and what pad properties are important in predicting polish performance. There is a need to design and manufacture an ideal pad that optimizes CMP and the whole IC manufacturing processes. The main features of an ideal pad are:

- Excellent lot-to-lot, pad-to-pad consistency
- Open pore structure improves slurry transport
  - Can operate at significantly lower flow rate
  - Better non-uniformity
- Open pore structure becomes easier to remove polishing residue
  - Lower defect
- Requires minimal break-in and conditioning
  - Reduce tool down time
  - Extend conditioner lifetime
  - Longer pad life

All the above-mentioned fact has directed us to investigate the bulk and nano scale mechanical properties of pad. The goal of this research is to address the materials and mechanics issues of IC 1000 pad.

The thesis is divided into four chapters. In Chapter 2, Quasi-static response (Elastic response) of the dry pad is examined (Experimental and analytical approaches have been devised). In Chapter 3, Dynamic response (Visco-Elastic response) of the dry pad and wet pad is examined (Experimental approach has been devised). The conclusions as well as recommendations for future work are presented in Chapter 4.

CHAPTER 2. QUASI-STATIC RESPONSE OF DRY PAD (ELASTIC RESPONSE)

2.1 Literature Review

Chemical Mechanical Polishing (CMP) has grown rapidly during the past decade as part of mainstream processing method in submicron integrated circuit manufacturing because of its global or near-global planarization ability. Currently, CMP is widely used for interlevel dielectrics and metal layer planarization [Martinez 1994]. The main objectives of CMP process are to planarize surface topography of dielectric deposits; to enable multilevel metallization and to remove excess deposited materials, which produces inlaid metal damascene structures and shallow trench isolations. A common way to perform the CMP process is by sliding the wafer surface on a relatively soft polymeric porous pad, flooded with chemically active slurry, containing abrasive particles of sub-micron diameter. The mechanical properties of the polishing pad and its surface morphology control the quality and efficacy of the CMP process. The pad surface morphology controls the partition of the applied down pressure between the abrasive particles and direct wafer/pad contact. The role of the pad is to distribute the slurry, support the wafer polishing pressure and support the shearing action of the slurry against the wafer surface while removing the polishing residues [Runnels et al 1994]. To aid slurry transport, the pad surface is either perforated (e.g., IC 1000 pad) or grooved (e.g., IC 1400). In this paper, we will focus on understanding the mechanical properties of a dry pad (IC1000 as a representative pad) and its response under the applied load. The gained insight would enable the optimization of the pad morphology that controls the abrasive particle interaction with the wafer surface and the quality of the resulting surfaces.

Polishing pads are composed of either a matrix of cast polyurethane foam with filler material or polyurethane felts to control its local hardness and long-range bending stiffness. In practice, it is not clear what pad property should be measured to characterize the polishing results. The pads as a cellular material is defined by its relative density, cell size, cell wall thickness, the degree to which the cells are opened or closed and their orientation [Gibson et al 1997]. In bulk foams, cellular materials present an initial elastic response due to cell wall bending and buckling, followed by a plateau stress corresponding to cell collapses and

densifications. Consistent with the range of pressures utilized in CMP, the pad is merely at its initial elastic response, where most of the deformation is limited to the surface asperity contact [Bastawros et al 2002]. In addition, the polishing pad behaves in elastic and/or visco-elastic manners under the applied pressure, which is thought to affect the within wafer non-uniformity (WIWNU) or planarity [Steigwald 1997]. It is observed that under relatively soft pads, small particles and low particle concentration, the pad undergoes local deformation, yielding an increased MRR with larger particle size and concentration. At the other extreme, the cell wall of individual pores within the pad deforms globally resembling a beam or plate, and a decreasing trend in MRR is observed with increasing particle size and concentration [Zhou et al 2002]. Motivated by such response, this paper will address the interplay between individual particle/pad contact and the local cell level deformation that would control the pad response.

Many models have been proposed to understand the complex behavior of the polishing pad during a CMP process. In these models, several features of the pad are considered, such as the stochastic distribution of pad asperity of various amplitudes and frequencies [Yu et al 1993], the pad local deformation at the particle scale [Fu et al 2001], the elastic asperity contact between the wafer and the pad [Luo et al 2001], as well as multi-level contact evolution at particle scale and the macro asperity scale, leading to several domains of wafer/particle/pad contacts [Bastawros et al 2002]. These models have shared the ambiguity in defining the proper pad mechanical property (e.g. Young's modulus and Poisson's ratio) as well as lumped up the influence of the pad surface morphology with the local abrasive particle contact.

The salient structural features of the pad (cell size, cell wall thickness & surface roughness) constitute structures that have several small length scales. The effect of these various length scales on the macroscopic mechanical response of the pad under different condition remains largely unexplored due to the deficiency of appropriate experimental techniques and testing protocols to characterize local deformation. To overcome these difficulties, we will utilize nanoindentation since it has been utilized extensively to probe elastic or visco-elastic local deformation characteristics within a relatively small volume of material. The advances in nanomechanical testing system have been made it possible to

continuously measure force and displacement as an indentation is made. The indentation load-displacement data thus derived can be used to determine mechanical properties at the sub-micron regime [Doerner et al 1986]. The developments in indentation testing methods and in modeling of the stress and displacement fields beneath the indenter gives a basis to study the spatial variations in local mechanical properties of the materials. The indentation of materials at nano- and micro-length scales enables in determining the local properties such as stiffness, hardness, elastic modulus, yield strength and fracture toughness. In the current study, a flat punch of $30\mu m$ radius and a conical tip of about $1\ \mu m$ radius will be employed to probe the pad cell membrane property at different length scales. The measured contact stiffness will delineate the interplay between the local particle level deformation and the cell level deformation and flexing.

2.2 Experiment

2.2.1 Sample used

An IC1000 dry pad without the sub pad is utilized in this study. The examined specimens where taken from a preconditioned pad that has been used in oxide CMP for 66 minutes at a pressure of 6 PSI and 120 RPM. The topography structure of the pad is shown in Fig. 2.1. It has a cellular structure with a cell diameter of $D_{cell} \approx 50-70\mu m$ and cell wall thickness of $t_{cell} \approx 3-5\mu m$. The locked-in porous structure with pined nodal points and semi-attached cell membrane faces produces higher initial stiffness and plateau stresses [Gibson et al 1997]. The details of pad surface roughness are evaluated with a surface profilometer at multiple length scales, relative to the pad cell diameter. There is a long wavelength roughness λ $(\lambda \approx 15-20D_{cell})$ with amplitude a, $(a \approx 0.1-0.2D_{cell})$ and within the roughness λ, there is a region λ_1 $(\lambda_1 \approx 2-4D_{cell})$ [Bastawros et al 2002]. The roughness λ and λ_1 (the region is marked by a dashed circle) is shown in Fig. 2.1. Within the local region, λ_1 the local cell surface roughness has a RMS in the range of 100-200nm and spatial periodicity of about 5-10 μm, as indicated in Fig. 2.2. A schematic representation of cell

diameter D_{cell}, cell wall thickness t_{cell}, long wavelength roughness λ and local cell surface roughness is shown in Fig. 2.2.

2.2.2 Indentation testing

Indentation tests were carried out using a Hysitron nanoindenter (TriboIndenter). The TriboIndenter is a stand-alone nanomechanical testing system, which has been designed to provide fully automated testing as well as in-situ imaging. Instrumented indentation tests consist of three basic components: (a) an indenter of specific geometry, (b) an actuator for applying the force, and (c) a sensor for measuring the indenter displacements. It has high-resolution instrumentation that can continuously control and monitor the loads and displacements of an indenter as it is driven into and withdrawn from a material. The sample is mounted on the XYZ stage of the TriboIndenter. The X and Y displacements of the stage and the optics of the TriboIndenter are used to locate an indentation region i.e., cell membrane of the porous pad. After locating the region the tip is moved for indentation. Mechanical properties are derived from the indentation load-displacement data. The resulting load-displacement data, together with the indenter geometry, can be analyzed to obtain hardness and elastic modulus using well-established, numerically verified mechanical models [Oliver et al 1992]. All tests were carried out under load control with loading and unloading rate of $100\mu N/s$ and hold time of 5 seconds at the maximum indentation load. The load-displacement plot during one complete cycle of loading and unloading is recorded to evaluate the contact stiffness. In this work, the contact stiffness is considered as the slope of the load vs. indentation depth curve during loading.

2.2.3 Indenters used

Two different indenter tips are utilized in this study, a conical tip and a flat punch (cylindrical indenter). Such selection is thought to provide the characteristics of the pad response at the particle scale, the initial pad cell-level multi-asperity contact as well as the local cell deformation. The geometry of the diamond conical indenter is shown in Fig. 2.3. The indenter has a 60^{o} half cone angle and a spherical nose radius of about $1\mu m$. The cone indenter has a sharp, self-similar geometry with a simple cylindrical symmetry that makes it

attractive from a modeling standpoint. In addition, the stress field associated with a conical indenter does not present any stress concentration similar to those associate with the edges of a pyramidal indenter. The second indenter is a stainless steel flat punch with a $30\mu m$ radius. The geometry of the indenter is selected to understand the contribution of the elastic cell membrane deformation on the macroscopic response of the pad. In addition, a circular flat punch can be easily approximated by the analytical response of a rigid axisymmetric flat-punch into elastic half space.

2.3 Experimental results

2.3.1 Conical Indenter Response (particle scale)

From the conical tip indentation, two distinct trends are observed. A typical load-indentation depth of conical tip for each trend is shown in Fig. 2.4 & 2.5. Trend-P1 (Fig. 2.4) shows three domain of deformation. (i) An initial soft response with a 200-350 N/m contact stiffness at a low applied load of 20-75μN. (ii) An increased contact stiffness of 400-550N/m as the applied load is further increased up to 90-225μN. (iii) Much higher contact stiffness is observed beyond this load limit and it approaches 500-650 N/m. Trend-P2 (Fig. 2.5) showed also three distinctive domains of deformations but at different level of indentation loads. (i) An initial soft response of 450-600 N/m for a range of loads of 50-200μN is observed. (ii) An increased contact stiffness of 600-800N/m up to a load of 200-400μN. (iii) A softer contact stiffness is followed of about 500-600 N/m. The observed creeping deformation at maximum load is due to the hold period before unloading. The final reduced modulus obtained from unloading curve is about 1.7 GPa, which is consistent with that of dense polyurethane.

It should be noted that the observed irrecoverable deformation after fully unloading is a visco-elastic deformation that would relax at a time scale much longer than the time scale of the experiment. The observed trend is quite repeatable except in some instances where a very compliant initial response has been observed, as noted in Fig. 2.6. Upon, multiple loading and unloading with a relaxation period of approximately 5 minutes, it has been observed that a steady state response is achieved. This trend was found to correlate with the existence of a local roughness with a higher frequency leading to a local radius of curvature much smaller than the indenter radius.

2.3.2 Flat Indenter Response (cell level)

Multiple indents are performed at different regions of the pad using the flat punch and a consistent trend of pad response is observed. Atypical load-indentation depth of the flat punch during one complete cycle of loading and unloading at different load levels is shown in Fig. 2.7. A three domain of deformation can be identified. (i) An initial soft response with continuously varying contact stiffness of about 500-1000 N/m at an applied load of 300-800μN. (ii) The contact stiffness approaches 1000-2000N/m up to loads of about 2000-3000μN. (iii) A harder response is observed with a contact stiffness of about 3500N/m. It is worth mentioning that the initial stiffness is about 3-5 times those observed in the conical indenter and marked by local indent for Trends-P1 and P2 as shown in Figs. 4 and 5. Moreover, the transition load between domains (i) to (ii) is about 3-6 times the corresponding transition loads for the same domains of Trend-P2 in Fig. 2.5.

2.3.3 Deformation Mechanisms

Multiple tests are carried out at different loads by using both the conical and the flat punch indenter. These tests showed the transition in the pad deformation characteristics. The speculated deformation mechanisms of the pad, based on the observed experimental trends are shown in Fig. 2.8. The deformation mechanism is derived from the observed change of contact stiffness at different applied loads in the nano-indentation experiments.

When a conical tip is used, because of smaller tip radius ($\approx 1\mu m$) the indenter initially touches or slides over a single or multiple asperities at low loads (Fig. 2.8-a). If the local asperity radius of curvature is greater than the indenter radius, the indenter settles over a single asperity, and the indentation field starts to evolve with the increased loading (Fig. 2.8-b). However, if the local asperity radius of curvature is smaller than the indenter radius, the indenter crushes multiple asperities, and thereby showing the reduced initial contact stiffness as indicated in Trend-P1 (Fig. 2.4) and from the multiple loading in Fig. 2.6. As the load is increased, a full contact between the indenter and the surface is established and indentation field start to evolve. At this stage, the process zone of the indentation is at least an order of magnitude less than the cell membrane thickness. As the load progress, the contribution of cell bending to the total deformation becomes more pronounced (Fig. 2.8-c).

When a flat indenter is used, high aspect ratio asperities with a wavelength much smaller than the indenter radius are crushed at low loads (Fig. 2.8-d). From the proportionality of the measured stiffnesses and transition loads of the conical and flat indenters, it seems there is about 2-5 high aspect ratio asperities are crushed within a single cell membrane. Such observation is consistent with the local asperity roughness measurements, shown in Fig. 2.1, where it is estimated to be about 4-6 asperities within the $30\mu m$ flat indenter radius. As the load is increased further the cell membrane bending contribution becomes significant (Fig. 2.8-e). Upon further increase of load, bulk response of the pad is observed (Fig. 2.8-f).

2.4 Modeling Pad Response

The experimental data showed a wide range of contact stiffnesses and transition loads associated with each of the presented deformation mechanisms. Such variation arises from the stochastic nature of the pad structure and its roughness. To understand this effect, the applied load-indentation depth for the range of observation is compared to those of the infinitesimal strain isotropic elastic response of spherical and conical Hertzian contact [Johnson 1999], as well as to the flexing of circular region (cell membrane) having fixed edges and loaded at the center. It should be noted that the utilized conical indenter has an initial round nose up to a depth of about 140 nm, shown in Fig. 2.3. Thus, for a shallow indentation depth, the applied load, F and the depth of penetration, h would be similar to a spherical indentation model for a sphere radius of, $r \approx 1\mu m$. Beyond a certain depth of penetration the F-h would follow that of the conical indenter with a semi cone angle, $\alpha = 60^{o}$. In the next section we will present the analytical results for a spherical indenter, conical indenter, flexing of a circular plate and then present a combined model of the pad response as shown in Fig. 2.9, which is compared to the experimental data. It should be noted that the bulk response under a singular load is thought to be outside the scope of this work, since in a CMP process, the global response of the long wavelength asperities dominates beyond the cell level [Bastawros et al 2002].

2.4.1 Spherical Indenter

The spherical indentation model for an elastic half space approximates the shallow depth response of the conical indenter at low loads, when the indenter is just touching the surface of the sample (Fig. 2.3). This behavior is expected in CMP when individual slurry interacts with the pad. From the Hertz theory and assuming an isotropic cell wall response, the elastic contact force between the pad and spherical indenter is given by [Johnson 1999],

$$F = \frac{4\,E_r\,r^{1/2}\,h_{sph}^{3/2}}{3} \tag{2.1}$$

Where r is the indenter radius, h_{sph} is the penetration depth and E_r is the reduce modulus$\left[1/E_r = \left(1-\nu_{pad}^2/E_{pad}\right)+\left(1-\nu_{indentor}^2/E_{indentor}\right)\right]$. Here E_{pad} and ν_{pad} are the Young's modulus and Poisson's ratio of the dense polyurethane, from which the pad is formed. For a nearly rigid indenter, $E_r \approx E_{pad}/1-\nu_{pad}^2$, Eq. (2.1) reduce to

$$F = \frac{4E_{pad}\,r^{1/2}\,h_{sph}^{3/2}}{3\left(1-\nu_{pad}^2\right)} \tag{2.2}$$

The Hertzian contact stiffness would follow from Eq. (2.2) as

$$K_{sph} = \frac{4E_{pad}\sqrt{r\,h_{sph}}}{3\left(1-\nu_{pad}^2\right)} \tag{2.3}$$

The contact stiffness is continuously evolving with the indentation depth, since the indentation process zone is expanding to encompass more material. The load vs. depth for $r = 1\mu m$ is plotted in Fig. 2.10 (spherical indent) by utilizing $E_{pad} = 1.7GPa$ and $\nu_{pad} = 0.5$ [Ward 1983].

2.4.2 Conical Indenter

The conical indentation model for an elastic half space approximates the higher depth response of the utilized conical indenter (Fig. 2.3). The elastic contact force between the pad and conical indenter is given by [Sneddon 1965],

$$F = \frac{2\,h_{con}^2\,E_{pad}\tan\alpha}{\pi\left(1-\nu_{pad}^2\right)} \tag{2.4}$$

Where α is the cone semi-angle, h_{con} is the penetration depth. The corresponding conical contact stiffness is given by,

$$K_{con} = \frac{2h_{con}E_{pad}\tan\alpha}{\pi\left(1-\nu_{pad}^2\right)} \tag{2.5}$$

In contrast with the spherical indentation stiffness, Eq. (2.3), the conical contact stiffness has a liner dependence on the indentation depth, or the indentation process zone is expanding at a slower rate, compared to the spherical case. The load vs. depth for $\alpha = 60^0$ is plotted in Fig. 2.11 (conical indent) by utilizing $E_{pad} = 1.7GPa$ and $\nu_{pad} = 0.5$ [Ward 1983] and the conical contact stiffness variation with indentation depth is plotted in Fig. 2.12 (conical indent).

2.4.3 Cell Bending

The porous polishing pad is composed of closed cells with varying cell size and cell wall thickness. Each intact cell-membrane (circled in Fig. 2.1) is assumed to be a circular plate with fixed edges and loaded at its center. For infinitesimal deformation, the force required to cause maximum deflection at the center of the plate is given by [Boresi et al 1985],

$$F = \frac{16\pi\, E_{pad}\, t_{cell}^3 h_{cell}}{3\left(1-\nu_{pad}^2\right) D_{cell}^2} \tag{2.6}$$

Where D_{cell} is the diameter of the circular plate, h_{cell} is the maximum deflection at the centre of the plate and t_{cell} is the thickness of the plate. The corresponding stiffness due to cell flexing is given by

$$K_{cell} = \frac{16\pi\, E_{pad}\, t_{cell}^3}{3\left(1-\nu_{pad}^2\right) D_{cell}^2} \tag{2.7}$$

The load vs. depth for $t_{cell} = 3.5\mu m$ and $D_{cell} = 50\mu m$ is plotted in Fig. 2.10 & 2.11 (cell bending) by utilizing $E_{pad} = 1.7GPa$ and $\nu_{pad} = 0.5$ [Ward 1983] and stiffness variation with depth which is a constant in plotted in Fig. 2.12 (cell bending).

2.4.4 Effective Pad response Model

The effective pad response can now be presented as the combined response of both the indentation and the cell membrane bending. The effective pad stiffness is evaluated from a

mechanical model of two-spring in series, sketched in Fig. 2.9. At shallow depth, the effective pad depth (total depth) h_{tot} is equal to sum of penetration depth, h_{sph} and the maximum deflection at the center of the plate h_{cell}.

$$h_{tot} = \left[\frac{3\left(1-\nu_{pad}^2\right)F}{4E_{pad}r^{1/2}}\right]^{2/3} + \frac{3\left(1-\nu_{pad}^2\right)D_{cell}^2 F}{16\pi E_{pad}t_{cell}^3} \qquad (2.8)$$

The effective pad stiffness, K_{eff} would be governed by both the spherical indentation stiffness, K_{sph} and the cell membrane flexing, K_{cell}. The effective pad stiffness is given by,

$$K_{eff} = \frac{F}{h_{tot}} \equiv \frac{K_{sph}K_{cell}}{K_{sph}+K_{cell}} \qquad (2.9)$$

The plot of indentation load, F vs. effective depth h_{tot} is shown is Fig. 2.10 (indent + bending). The prediction of Eq. (2.8) is compared to the experimental data range at low loads in Fig. 2.10. For this comparison, the employed model plate dimensions were $t_{cell} \approx 3.5\mu m$ and $D_{cell} \approx 50\mu m$. The property of the dense polyurethane was $E_{pad} = 1.7GPa$ and $\nu_{pad} = 0.5$. It is quite remarkable that the experimentally measured data range at low indentation loads fall between the effective pad response model employing the combined effects of local spherical indentation and cell bending.

At large indentation depth when the conical indentation field dominates, the effective pad depth (total depth), h_{tot} is equal to sum of penetration depth, h_{con} and the maximum deflection at the center of the plate h_{cell}.

$$h_{tot} = \left[\frac{\pi\left(1-\nu_{pad}^2\right)F}{2E_{pad}\tan\alpha}\right]^{1/2} + \frac{3\left(1-\nu_{pad}^2\right)D_{cell}^2 F}{16\pi E_{pad}t_{cell}^3} \qquad (2.10)$$

The effective pad stiffness, K_{eff} would be governed by the conical indentation stiffness, K_{con} and the cell membrane flexing, K_{cell}. In this range, K_{eff} is given by

$$K_{eff} = \frac{F}{h_{tot}} = \frac{K_{con}K_{cell}}{K_{con}+K_{cell}} \qquad (2.11)$$

The plot of indentation load, F vs. effective depth h_{tot} is shown is Fig. 2.11 (indent + bending). The prediction of Eq. (2.10) is plotted with the range of the experimental data in Fig 2.11. Similar material properties and cell membrane dimensions to those in Fig. 2.10 are utilized. The experimental data is represented by the average of 10 indentation tests carried at different spatial positions for each loading level, with the horizontal scatter bar showing the data range. This scatter bar is due to stochastic variation of the pad cell surface morphology and cell dimensions. Apparently, the effective pad response model (based on the combination of local conical indentation and cell bending) lies well within the experimental data. The effective pad stiffness, K_{eff} variation with depth from Eq. (2.11) is plotted in Fig. 2.12 (indent + bending).

2.5 Discussion

The various experimentally observed trends can be understood in view of the pad surface morphology and the deformation mechanisms depicted in Fig. 2.8. When a conical indenter is used with a tip radius in the same range of the abrasive particle size employed in CMP, the measured macroscopic response is a combination of the local cell membrane roughness and the local cell flexing response. The initial soft Trend-P1 shown in Fig. 2.4 arises from the interaction of the tip with the local roughness, wherein the tip of the indenter is just establishing the surface contact over sub-micron asperities or sliding over a single asperity. Such interaction would reduce the initial contact stiffness and limit it below 350N/m. As the load is progressively increased the tip starts to locally indent the pad cell membrane and thereby increasing the contact stiffness to the range of about 550N/m. It is noted that the contact stiffness should not be constant in view of simple spherical Hertzian contact [Johnson 1999], wherein the contact stiffness has a square root dependence on the indentation depth. As the load is further increased, the cell wall starts to globally deflect in bending. Once the cell wall bending dominates, the macroscopic observable contact stiffness will be reduced and follow that of the cell wall flexing. The Trend-P2 in Fig. 2.5 is consistent with an initiation of a local cell indentation at the start of loading followed by a global cell wall bending at the same range of transition load as those of Trend-P1. As the load is further

increased beyond 400μN, the bulk response of the pad starts to influence the macroscopic response and thereby decreasing the contact stiffness further.

The observed trend from the flat punch of 30μm radius complements the local measurements by the conical tip. The presented trend in Fig. 2.7 for flat punch at high loads represents initial multiple asperity contact with a range of continuously varying contact stiffness of 500-1000N/m. This level of contact stiffness is consistent with the observed trend of contact stiffness variation from the single asperity indentation manifested by the local conical indention of the cell membrane, Fig. 2.4 & 2.5. This can be understood if one considers the local roughness of the cell membrane (Fig. 2.1 & 2.2) there would be about 4-6 asperities below the flat punch indenter. Thus the effective initial contact stiffness of the flat punch would be the sum of contact stiffness of individual asperity (~ 200-350N/m), which is equivalent to a set of springs in parallel. The corresponding applied load per asperity would be about 50-100μN, which is consistent with the transition load for the single conical indentation. The following increase of contact stiffness to the range of 1000-2000N/m is consistent with global bending of the cell membrane. Such consistency between the results of the two indenter's configuration supports the proposed cell bending mechanism. Finally, the contact stiffness reaches that of the bulk of about 1500-3500N/m at a load range of 1500-3500μN.

At shallow depths, where the tip radius influences the relation between the load and depth of penetration, the combined model (spherical indent + cell bending) lies well within the experimental measurements range proving the validity of this model (as shown in Fig. 2.10). So the spherical Hertzian contact model is used along with cell bending model to form a series spring mechanical model at shallow depth. At higher depths, where the semi cone angle influences the relation between the load and depth of penetration, the combined model (conical indent + cell bending) lies well within the experimental measurements range (as shown in Fig. 2.11). So the conical Hertzian contact model is used along with cell bending model to form a series spring mechanical model at higher depth. To understand which of the above models (conical Hertzain contact model / cell bending model) dominates, effective pad stiffness K_{eff} vs. depth plot is necessary (Fig. 2.12). The effective pad stiffness K_{eff} (indent + bending) curve as shown in Fig. 2.12 is linear at lower depth, which indicates that conical

Hertzain contact model (local indentation) dominates. As the depth increases the curve becomes non-linear, this represents gradual switching of conical indentation to cell bending. At higher depth the curve becomes flat which clearly represents that the cell bending is substantial.

The presented experimental data and the proposed model lays a foundation for modeling the material removal rate and defect evolution during the CMP process. It is now clear that the whole CMP process is controlled by the evolution of the pad surface deformation and to a much lesser extent by the pad bulk response. From the flat indenter results of Fig. 2.7, and by incorporating the effective contact area ratio [Bastawros et al 2002] over the long wave length λ, the equivalent applied load on the pad that corresponds to a 5000mN load on individual cell is about 10kPa and the corresponding average strain at this load is about 0.5%. This value of average strain represents about 25% of the speculated pad compressibility during a standard CMP operation. A major portion of the load partitioning and redistribution is controlled by the surface morphology and deformation characteristics of the pad surface. Therefore, the provided characterization of the pad at the cell level as well as the proposed effective stiffness model would provide more realistic approach for accounting for the pad stiffness when accounting for the transfer of the applied pressure to local forces on individual abrasive particles. In addition, the proposed model would provide a systematic way to understand the effect of varying the local and global pad stiffness on defect evolution (scratches at particle scale or defects at die scale) like dishing and erosion.

The quasi-static analysis of a dry pad provides some understanding of the cell-level pad deformation characteristics; further work is needed to understand the pad dynamics, viscoelastic effects and the role of water adsorption on cell level and macroscopic properties. Further work is currently underway to address these effects [Gouda et al 2004].

2.6 Summary

- The deformation mechanisms at the pad cell level have been studied experimentally.
- It is found that the macroscopic pad response is controlled by both the local indentation of the pad cells as well as the flexing deformation of the cell wall.

- The experimentally observed trends from quasi-static tests and deformation mechanisms indicate that the whole CMP process domain is carried out by local pad cell level interaction at the contact interface and not by the bulk response of the pad.
- The force-displacement plot obtained from the elastic response of the pad by quasi-static tests matches well with the series- spring mechanical model.
- The spherical Hertzian contact model is used along with cell bending model to form a series spring mechanical model at shallow depth and the conical Hertzian contact model is used along with cell bending model to form a series spring mechanical model at higher depth.
- It is also observed that cell bending is substantial as compared to local indentation at higher depths.

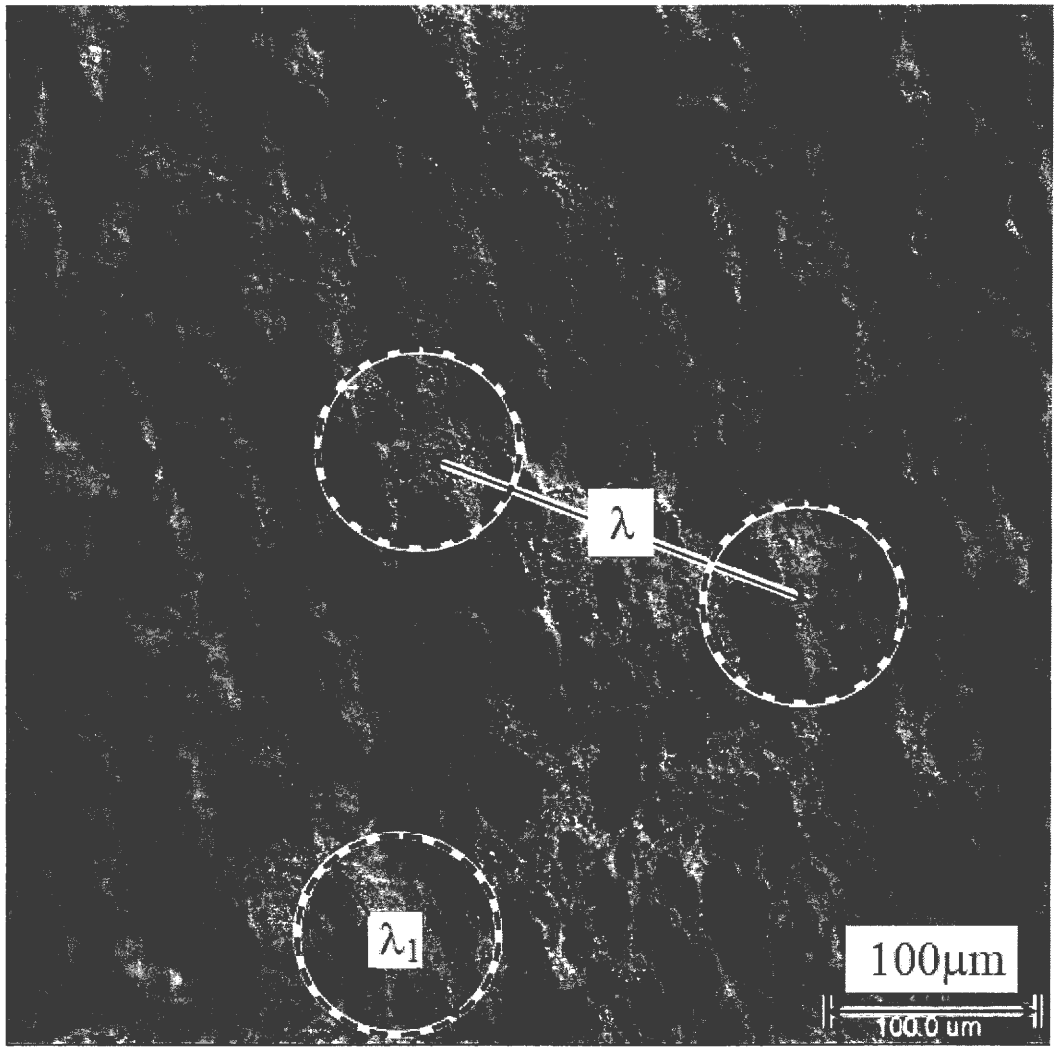

Figure 2.1: SEM image of a preconditioned pad surface morphology (IC1000). The dashed circles show the long wavelength roughness λ $\left(\lambda \approx 15-20D_{cell}\right)$ with a higher summit of length λ_1 $\left(\lambda_1 \approx 2-4D_{cell}\right)$

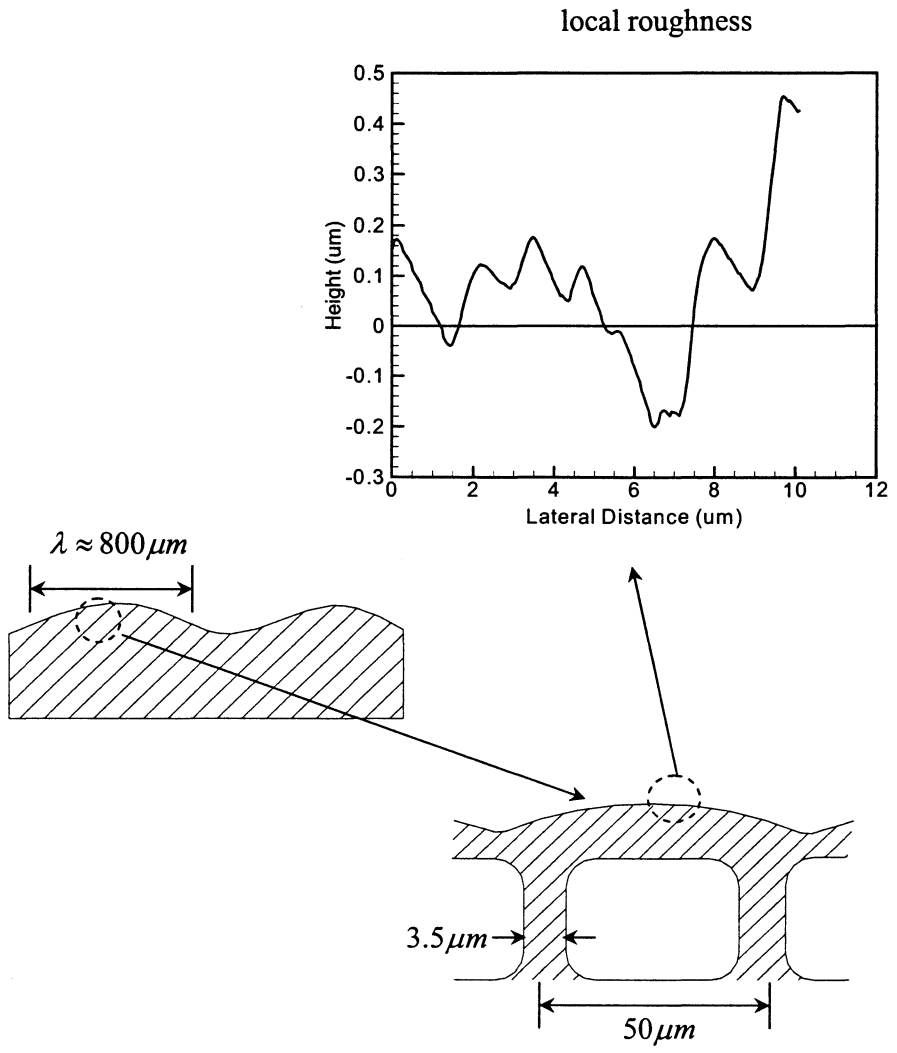

Figure 2.2: Illustration of pad morphology at different length scales

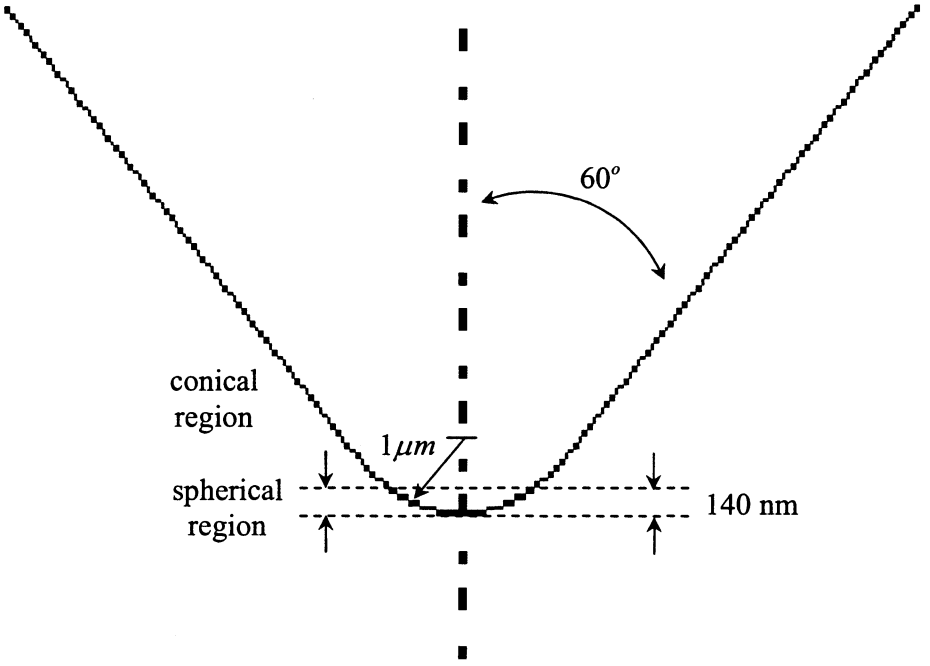

Figure 2.3: Schematic representation of the utilized conical indenter

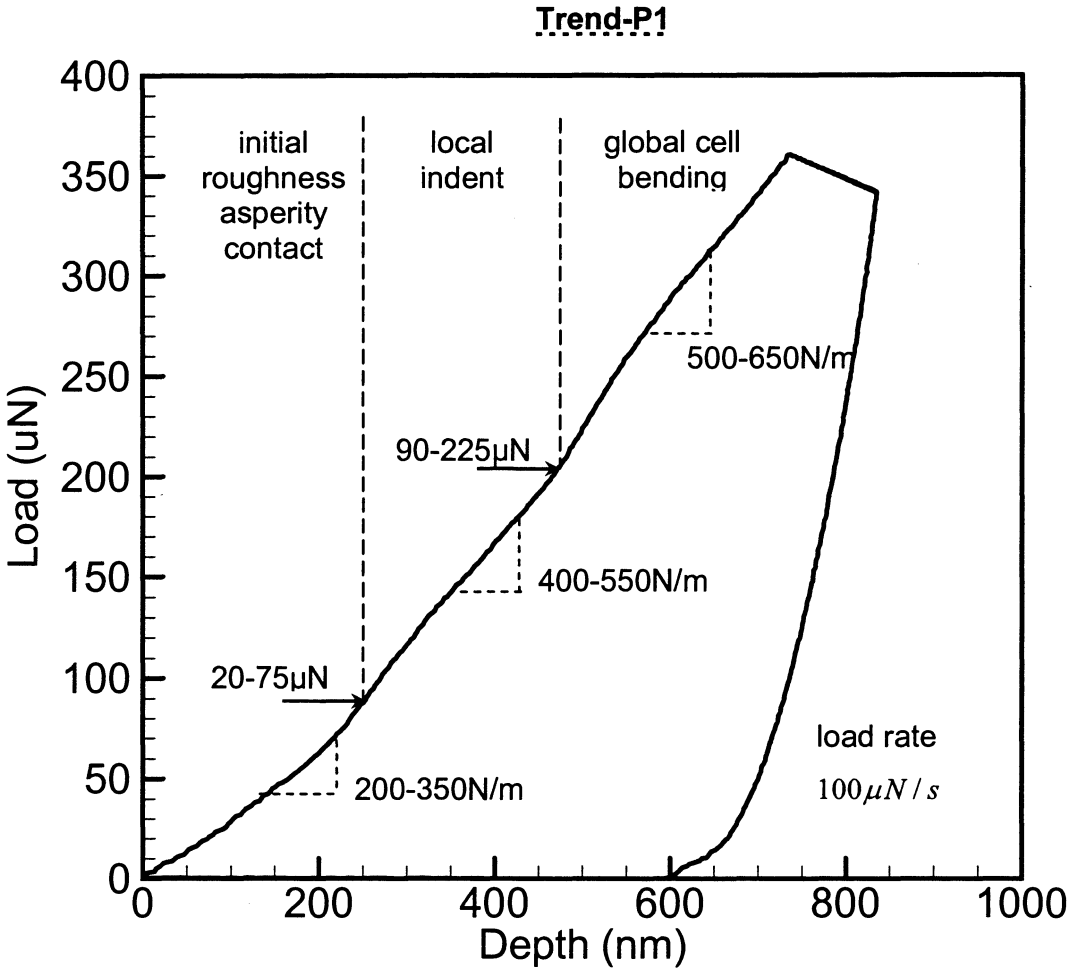

Figure 2.4: Load-indentation depth curve using conical indenter showing Trend-P1

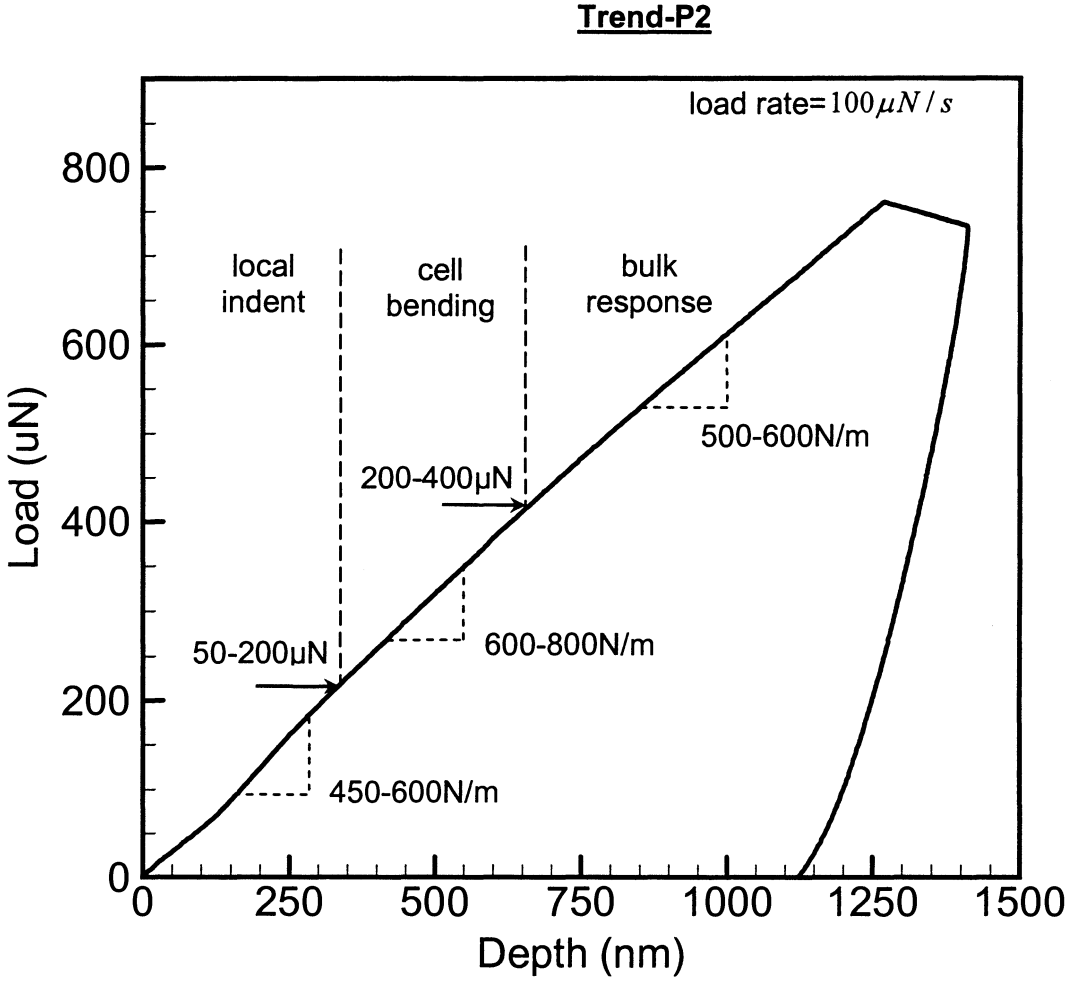

Figure 2.5: Load-indentation depth curve using conical indenter showing Trend-P2

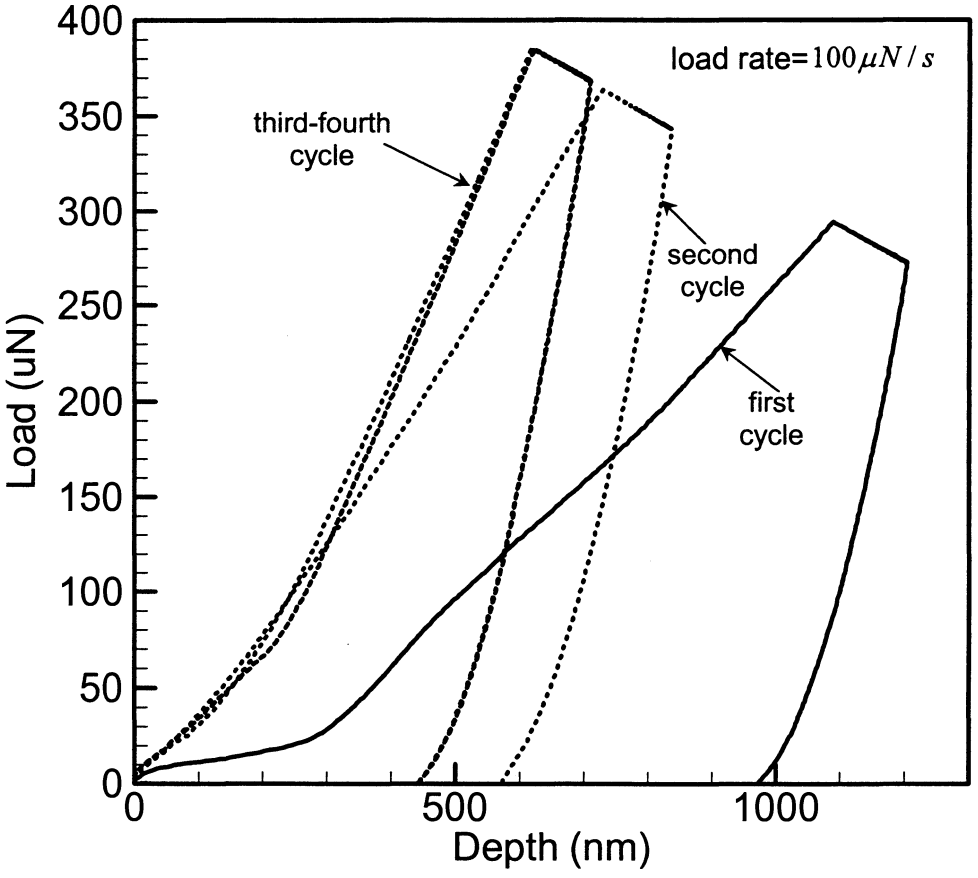

Figure 2.6: Multiple loading and unloading with a relaxation time of 5 minutes

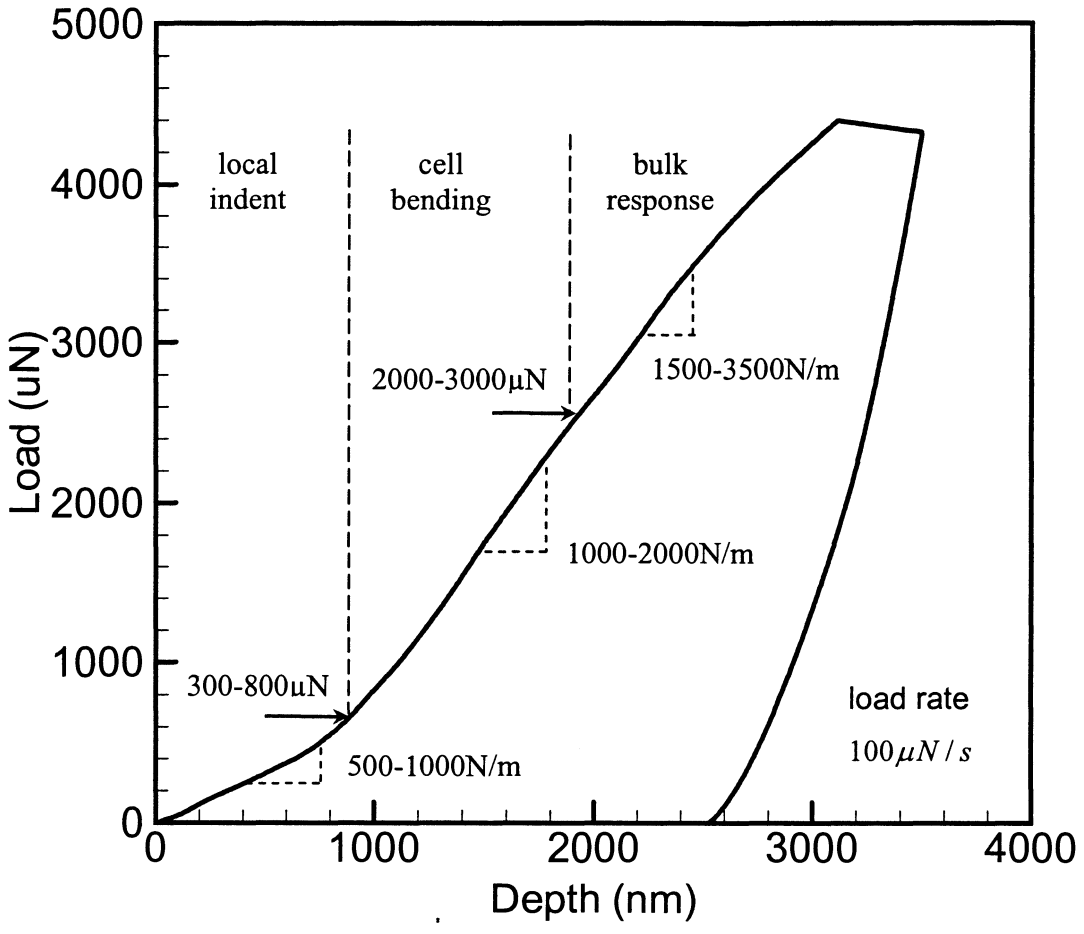

Figure 2.7: Load-indentation depth using a flat punch (cell level)

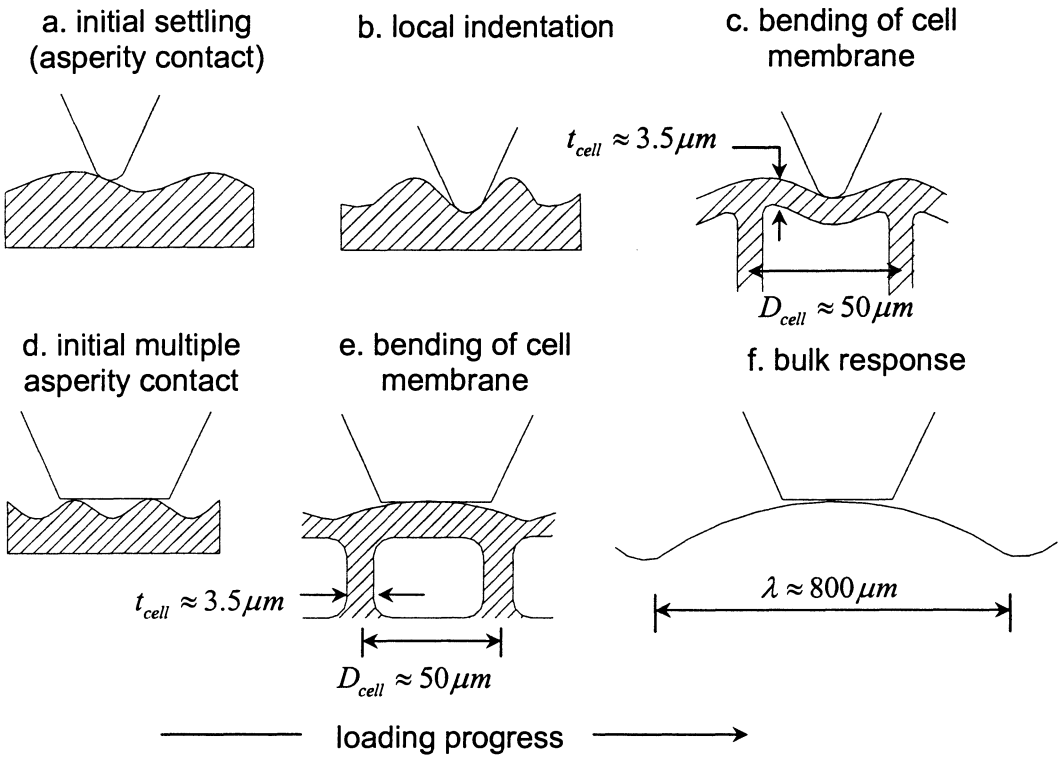

Figure 2.8: Pad deformation mechanism for conical and flat indenters

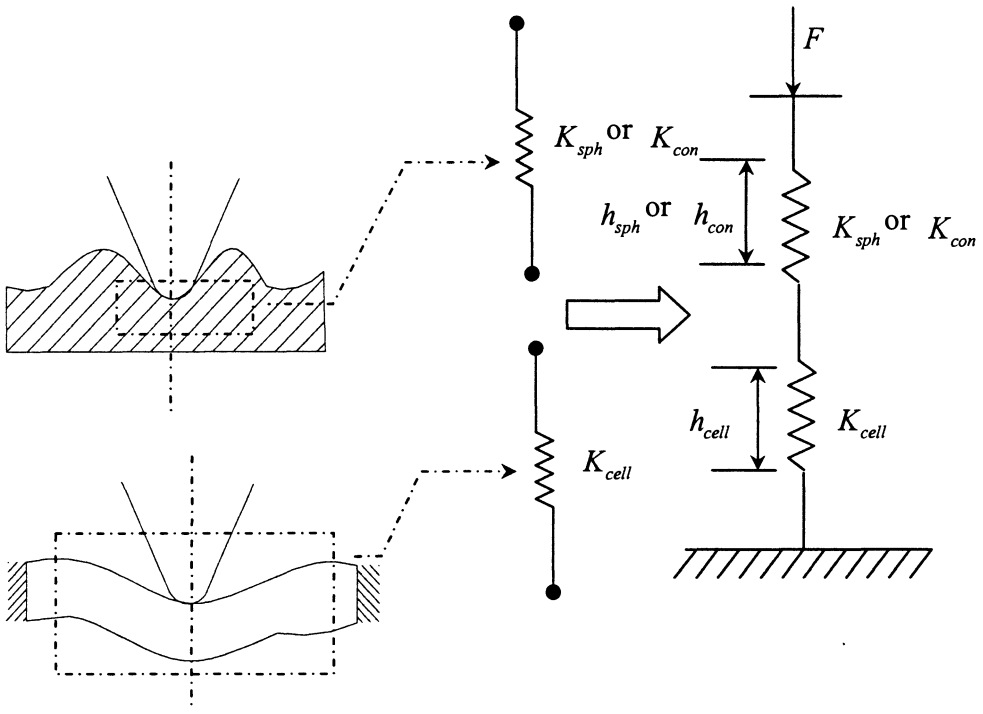

Figure 2.9: Series spring mechanical model for force-controlled indentation assuming purely elastic response

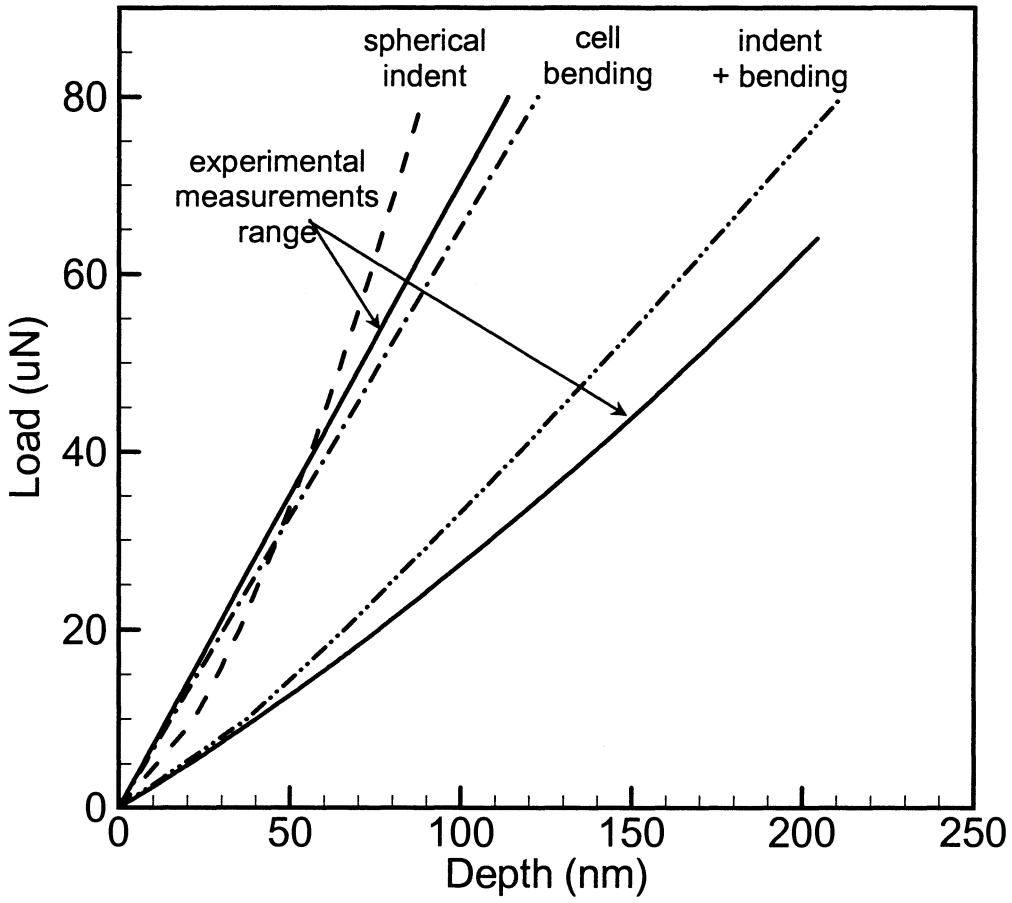

Figure 2.10: Comparison of experimental data range with series spring model for elastic deformation of pads at shallow depth (indenter spherical region)

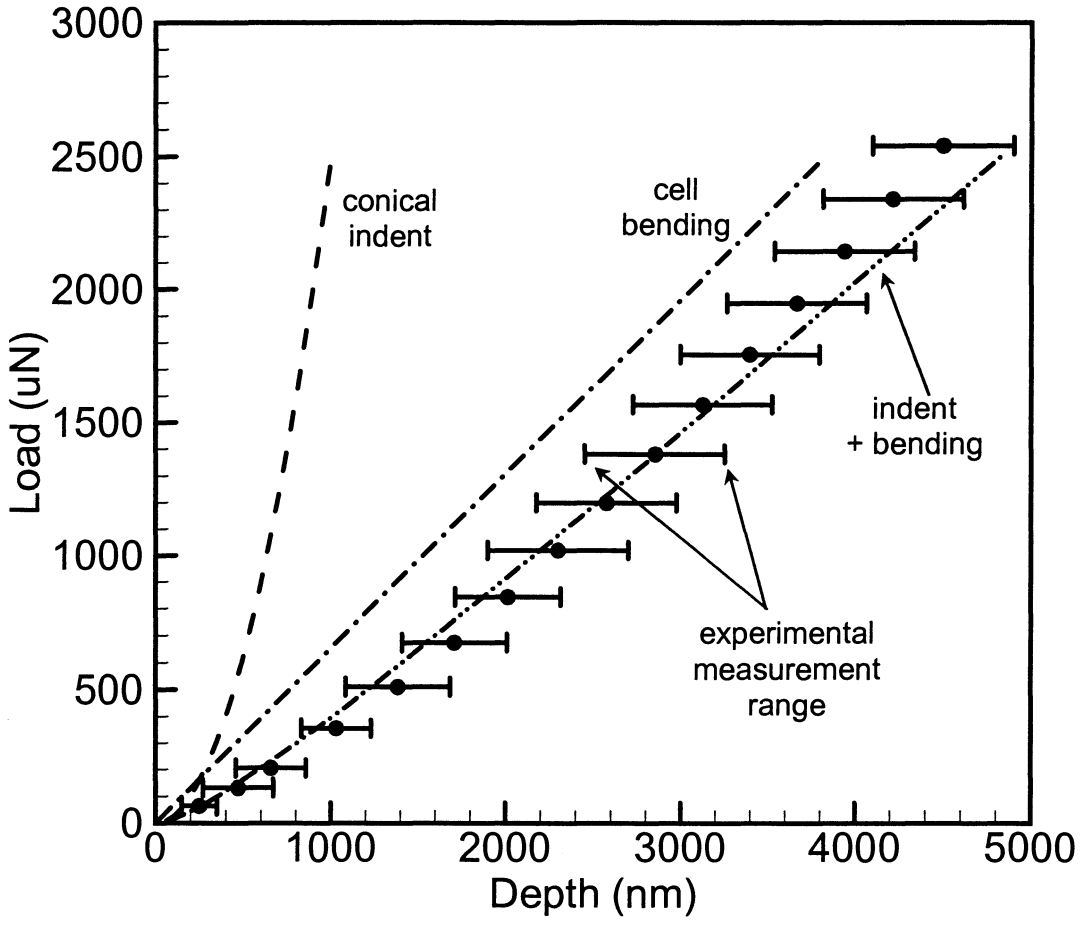

Figure 2.11: Comparison of experimental data range with series spring model for elastic deformation of pad at higher depth (indenter conical region)

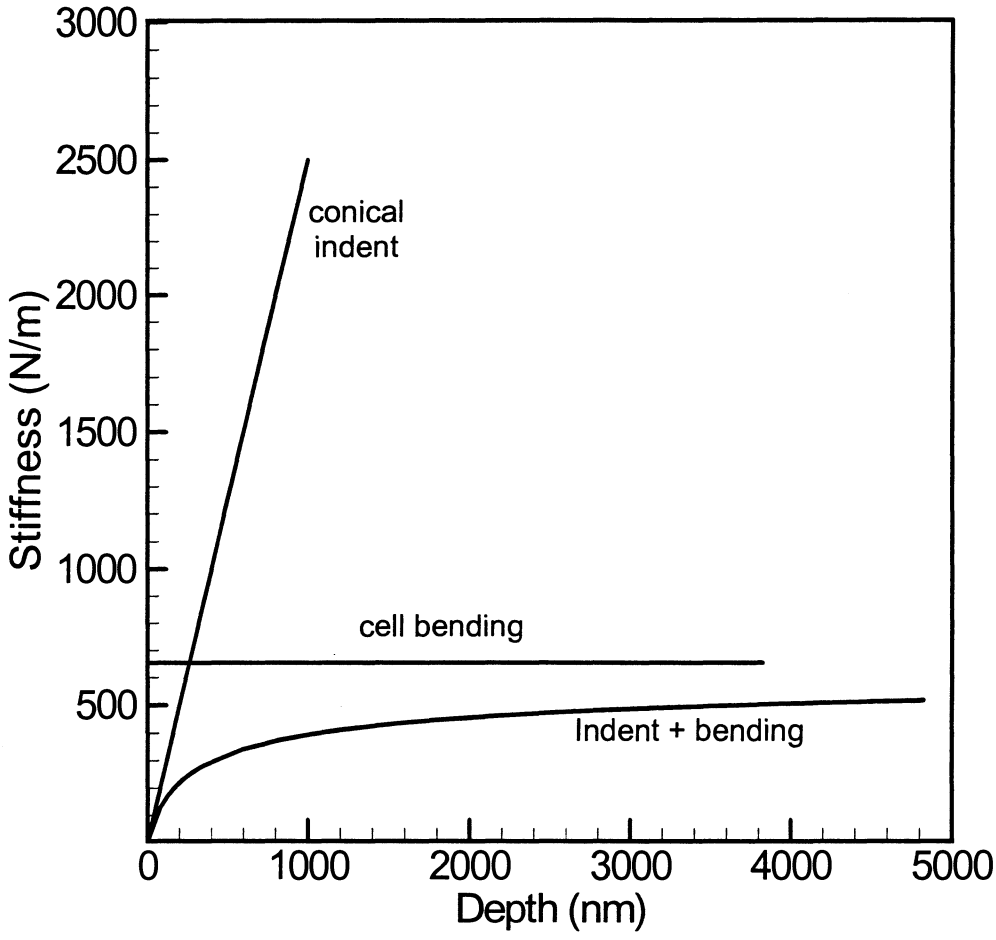

Figure 2.12: Variation of different stiffness with indentation-depth for elastic deformation of pad at higher depth (indenter conical region)

CHAPTER 3. DYNAMIC RESPONSE OF WET AND DRY PAD (VISCO-ELASTIC RESPONSE)

3.1 Literature Review

Chemical mechanical polishing (CMP) has emerged as a critical process among the newly developed planarization technologies for ultra large-scale integration metallizations. During the CMP process, a silicon wafer is faced side down on a compliant surface (polishing pad) under high pressure and slurry consisting of fine abrasives and chemical is passed in between. Even though the process looks simple, CMP is a complicated process in which both mechanical and chemical factors play an important role. Many researchers have tried to address various aspects of CMP process like influence of abrasive size distribution [zhou et al 2002, luo et al 2003], multi-scale pad properties [Bastawros et al 2002, Gouda et al 2004], interfacial pressure [shan et al 2000] and fluid hydrodynamics [Runnels et al 1994]. Among all these aspects of CMP, polishing pad is a critical component of the CMP process.

The main role of polishing pad is to hold the abrasive particles intact so that it enables the machining operation, distributes the slurry, support the wafer polishing pressure and transfer the load to the abrasives. Izumitani (1979) found that to satisfy these requirements, the pad must be viscoelastic so that the polishing grain can be embedded and at the same time, it has to be rigid enough to transmit the load. In other words, pad should have viscoelastic characteristics and is generally made of polymeric materials such as polyurethane for CMP pads. The viscoelastic deformation of the pad also plays an important role in the planarization process. As the wafer transverses the pad surface according to its kinematic design, high areas and low area, it cannot deform immediately due to viscosity so that less pressure is on the low area. On the other hand, as the pad passes from a low area to a high area, it cannot conform immediately to the high area so that a higher pressure is on the high area. From this prospective, viscosity of the pad improves the planarization efficiency. However, it is undeniable that some inherent problems associated with the polishing pad are responsible for time-dependent and non-uniform material removal, which results in dishing and erosion problems. It is speculated that these problems have a lot to do with the pad deformation mechanism [Gouda et al 2004], pad surface morphology [Bastawros et al 2002],

time dependent behavior of pad [Fu et al 2002], cellular structure [Gibson 1997] of pad and effect of pad soaking [Ng et al 2003].

The polishing pad is made of a foamed polyurethane material containing randomly distributed pores or cells. The salient structural features of the pad (cell size, cell wall thickness & surface roughness) constitute structures that have several small length scales. In the prior work [Gouda et al 2004] we examined the multi-scale response of dry IC-1000 pad using nano-indenter in quasi-static model and examined different deformation mechanism along with a simple analytical model for the effective elastic stiffness. From the insight gained by the previous work we extend our work to understand the dynamics of pad (viscoelastic effects) and role of water adsorption on its cell level and macroscopic properties. This work was possible due to the advancement in nanomechanical testing system developed by Hysitron Inc. and the development of force modulation technique using a capacitive load displacement transducer [Syed Asif et al 1998]. In this paper an experimental procedure is used to study the dynamic response of a foamed polyurethane material at different frequencies and depths.

3.2 THEORY

In the AC force modulation technique, a small sinusoidal ac force is superimposed on the dc-applied load. The resulting oscillation in displacement is monitored using the two-channel lock-in amplifier. The amplitude and phase shift can be used to calculate the contact stiffness using a dynamic model [Pethica et al 1987]. The indenter and contact are represented by the components in the dynamic model as shown in Fig. 3.1.

The amplitude of the displacement signal is [Pethica et al 1987]

$$X = \frac{F}{\sqrt{\left(k - m\omega^2\right)^2 + \left[\left(C_i + C_s\right)\omega\right]^2}} \tag{3.1}$$

and the phase shift between force and displacement is

$$\phi = \tan^{-1}\frac{\left(C_i + C_s\right)\omega}{k - m\omega^2} \tag{3.2}$$

where F is the ac force amplitude, m is the indenter mass, ω is the frequency in rad/s, C_i is the damping coefficient of the air gap in the displacement sensing capacitor, C_s is the

damping coefficient of the specimen and the combined stiffness of the contact and the indenter supporting spring is given by

$$k = K_s + K_i \tag{3.3}$$

K_s is the stiffness component in phase with the applied force, that is the storage component and ωC_s is the loss component of the stiffness. If both the components of the stiffness are known then the storage modulus E' and loss modulus E'' can be obtained from the stiffness equations [Oliver et. al 1992]

$$K_s = 2\sqrt{\frac{A}{\pi}}E' \tag{3.4}$$

$$\omega C_s = 2\sqrt{\frac{A}{\pi}}E'' \tag{3.5}$$

where A is the contact area, which can be calculated by the expression,

$$A = c_o h_c^2 + c_1 h_c + c_2 h_c^{1/2} + c_3 h_c^{1/4} + c_4 h_c^{1/8} + c_5 h_c^{1/16} \tag{3.6}$$

where $c_o, c_1, c_2, c_3, c_4, c_5$ are constants, which depend on the shape of the indenter, and h_c is the depth of indentation.

In this work, a simple mechanical Voigt model represents a polymeric system. In this model, the viscoelastic component of the contact is described by a linear spring of stiffness K_s in parallel with a dashpot with damping coefficient C_s. The relaxation time of the polymer surface associated with its viscoelastic response is given by,

$$\tau = \frac{C_s}{K_s} \tag{3.7}$$

The loss tangent of the material is defined as the ratio of the loss modulus (E'') to the storage modulus (E'), which is equivalent to

$$\tan\delta = \frac{C_s\omega}{K_s} \tag{3.8}$$

The loss tangent determines the macroscopic physical properties as the damping of free vibrations, the attenuation of propagated waves, and the frequency width of resonance response. It can often be more conveniently measured than any other viscoelastic function.

3.3 Experiment

3.3.1 Sample used

An IC1000 dry pad without the sub pad is utilized in this study. The examined specimens where taken from a preconditioned pad that has been used in oxide CMP for 66 minutes at a pressure of 6 PSI and 120 RPM. The topography structure of the pad is shown in Fig. 3.2. It has a cellular structure with a cell diameter of $D_{cell} \approx 50-70\mu m$ and cell wall thickness of $t_{cell} \approx 3.5-6\mu m$. The details of pad surface roughness are evaluated with a surface profilometer at multiple length scales, relative to the pad cell diameter. There is a long wavelength roughness λ $(\lambda \approx 15-20D_{cell})$ with amplitude a, $(a \approx 0.1-0.2D_{cell})$ and within the roughness λ, there is a region λ_1 $(\lambda_1 \approx 2-4D_{cell})$ [Bastawros et al 2002]. The roughness λ and λ_1 (the region is marked by a dashed circle) is shown in Fig. 3.2. The local cell surface roughness has a RMS in the range of $0.5-2\mu m$ and spatial periodicity of about $15-20\mu m$ [Gouda et al 2004] as shown in Fig. 3.2. Wet samples are prepared by soaking the pad in water for one hour and then air is blown on the surface so that no water droplet stays on the surface.

3.3.2 Indentation tests

Indentation tests were carried out using a Hysitron nanoindenter (TriboIndenter). The TriboIndenter is a stand-alone nanomechanical testing system, which has been designed to provide fully automated testing as well as in-situ imaging. The sample is mounted on the XYZ stage of the TriboIndenter. XY displacements of the stage and the optics of the TriboIndenter are used to locate an indentation region i.e., cell membrane. After locating the region the tip is moved for indentation. Mechanical properties are derived from the indentation load-displacement data obtained from the tests. Conical diamond indenter with a 60° half cone angle with a spherical nose radius of about $1\mu m$ is used. The schematic representation of conical indenter is shown in prior work [Gouda et al 2004].

Using this instrumented indentation machine two types of tests are done on wet and dry pad samples:

a. Quasi-Static tests (DC Technique)

For depth-sensing nanoindentation, a controlled, variable force is applied to a sample by the indenter and the resulting displacement of the indenter is measured. A single indent is done using an indenter of specific geometry (conical tip) for a desired load function. In all the quasi-static tests a trapezoidal load function is used. A trapezoidal load function has three segments, (i) the load increases linearly with time till the maximum is reached (this segment is also called as loading cycle) (ii) the maximum load is held constant for some time (iii) the load is decreased linearly with time (this segment is also called as unloading cycle). This test is useful in understanding the material response during loading and unloading cycles. The indentation load-displacement data during one complete cycle of loading and unloading is recorded, to evaluate the contact stiffness. The contact stiffness is defined as the segmental slope of the load-indentation displacement curve.

b. Dynamic tests (AC Modulation Technique)

The nanoDMA technique developed at Hysitron, Inc. has been used to obtain much more information about the sample. For visco-elastic materials, it is very difficult to obtain meaningful and accurate data using quasi-static testing. This technique overcomes the insufficiencies in the legitimacy of quasi-static testing for materials that display significant time-dependent deformation and recovery. Dynamic methods allow for the continuous measurement of stiffness as the indenter is driven in during loading. The measurement is done by, superimposing a small force oscillation on the primary loading signal and analyzing the resulting displacement response by means of a frequency-specific amplifier. The phase difference between the displacement signal and the force signal can also be measured. With dynamic stiffness measurement, one can obtain the stiffness, hardness and elastic modulus as a continuous function of depth from a single indentation experiment. Since the sample (IC 1000 pad) used is a visco-elastic material, dynamic test is found to be very useful to obtain the time-dependent material properties. Quantification of the data depends on obtaining accurate dynamic characterization of the instrument (dynamic response vs. frequency), and applying an appropriate dynamic model [Pethica et al 1987]. A ramping quasi-static test is done on the pad samples, where the dynamic load is held to a fixed percent of quasi-static load as it is changed. The dynamic load function is set up using segment. In each segment the

indentation parameters, i.e., loading rate, frequency and amplitude of the ac force; sensitivity and time constant of the lock-in amplifier can be set individually. The quasi-static load is increased linearly while the dynamic load is increased to a fixed percent of quasi-static load at each step and the frequency applied is held constant (50Hz). A ramping frequency test is also done on the pad samples, where the frequency is varied with a constant quasi-static and dynamic load, to obtain the visco-elastic properties of the material.

3.4 Results and Discussion

To understand the dynamics of a dry pad, a ramping frequency test is done by applying a constant quasi-static load ($P = 1000\mu N$) and a constant dynamic load ($100\mu N$). Figure 3.3 shows the plot for the ratio of harmonic displacement (X) over the amplitude of the harmonic force (F) as a function of frequency for load of $1000\mu N$ on a cellular membrane of the IC 1000 pad. This figure shows that at low frequencies, below 100Hz, (X/F) is decreasing as a function of frequency while for fused silica (no damping) the ratio of (X/F), remains constant as a function of frequency [Loubet et. al 2000]. This decrease is indicative of viscoelastic behavior of the IC 1000 pad sample.

Figure 3.4 shows the evolution of the loss tangent (Eq. 3.8) as a function of frequency. The Loss tangent, which is dimensionless, is a useful parameter and conveys no physical magnitude but is a measure of the ratio of energy lost to energy stored in a cyclic deformation. At low frequencies, $\tan\delta$ is large for all the uncross-linked polymers and in fact becomes inversely proportional to the frequency. Figure 3.4 represents a plateau zone [Ferry 1980] and the characteristic feature of the plateau zone is that the magnitude E'' is smaller than that of E'. In the plateau zone, the loss tangent thus passes through a minimum; the losses are small here because the period of oscillation is long compared with the longest relaxation time of an entanglement network strand but short compared with any relation times of motions involving entanglement slippage. It also shows that the acquired points are between the α and β relaxation of the polymer. The left side of the curve, below 50Hz, belongs to the α peak. The right side of the curve, greater than 100Hz, belongs to the β peak.

Figure 3.5(a) and 3.5(b) shows the variation of response time τ (Eq. 3.7) and contact stiffness K_s with the frequency for a constant load of $1000\mu N$. The reduction in response time was accompanied by an increase in the contact stiffness; this is because as frequency increases the contact becomes more glassy, as observed for the bulk [Ferry 1980].

Figure 3.6(a) shows the stiffness-depth trend obtained from indenting on different cells (dashed circles shown in Figure 2) of the IC 1000 pad. The contact stiffness is obtained from equations 3.1-3.3. Since the contact stiffness is known the damping coefficient of the specimen material can be calculated from the equations 3.1-3.2. Figure 3.6(b) shows the variation of the damping coefficient as a function of depth of penetration. It is interesting to note that variation of contact stiffness and the damping coefficient with penetration depth is non-linear. This contradicts the fact mentioned in [Syed Asif et al 1998] where the stiffness and damping variation with depth is linear in a Poly-cis-isoprene specimen. The possible explanation for this non-linearity is due to the fact that is a combination of local indentation and cell bending [Gouda et al 2004] of the cell membrane.

The storage modulus E' can be calculated from the stiffness-depth data using equation 3.4. The variation of reduced modulus or storage modulus E' with depth is plotted in Fig. 3.7. It is observed that the value of E' drops with depth while in bulk polymers and metals E' is constant with depth. The possible explanation can be justified using the concept mentioned by [Kovalev et al 2004]. 'When a bi-layered system with a stiff layer above a compliant layer is indented, the effective reduced modulus drops as the depth of indentation is increased. So for our sample (foamed polyurethane), effective reduced modulus drops because of the combination of local indentation (stiff) and cell bending (compliant).

To justify further why the storage modulus E' drops with depth of indentation, which contradicts the trend observed in any bulk polymer [Syed Asif et al 1998] a different approach is followed. First, assume a constant value of storage modulus $E' = 1.5GPa$. Second, calculate the value of K_s at each depth from Eq. 3.4 & Eq. 3.6. Third, plot the value of K_s at each depth of indentation. Fourth, plot the contact stiffness values at each depth obtained from the indentation. The variation of K_s by using Eq. 3.4 & Eq. 3.6 is linear with depth while the variation of K_s is non-linear with depth from experiments. So if one

compares Fig. 2.12 and Fig. 3.8 (experimental data) the non-linear stiffness is accounted for a combination local indent and cell bending. The difference in magnitude as observed in Fig. 2.12 and Fig. 3.8 (experimental data) is because one is loading contact stiffness and the other is unloading contact stiffness. This justifies the dropping reduced modulus, storage modulus and loss modulus with depth is due the cell bending.

Figure 3.9 shows the variation of stiffness with depth at different frequencies (10, 50, 100, 200 Hz). It is seen that as the frequency is increased the variation stiffness with depth is increased. The response of a single cell (dashed circles shown in Figure 2) of IC 1000 pad at different frequencies could be used to explain some intricate problems like non-uniform material removal rate, dishing and erosion in the CMP process. This trend might by useful for the pad manufactures since it describes the dynamics and visco-elastic behavior of the pad.

In this work an attempt is also made to study the response of a wet pad. An indent is made on a particular dry cell membrane and the tip is withdrawn. The pad is soaked for one hour putting a water droplet on the pad surface. After an hour air is blown to ensure that there is no water drop-let on the surface and then an indent is made on the same location. The response of a dry and wet cell membrane is shown in Figure 3.10 (loading & unloading cycle), Figure 3.11 (loading curve at 50Hz) and Figure 3.12 (contact stiffness at 50Hz). In all these trends it is seen that the wet cell membrane shows lower stiffness because of softening of material due to water absorption.

The Quasi-Static response of the cell membrane in dry and wet condition is obtained by applying a trapezoidal load function (a linear loading rate of $100\mu N/s$, a hold for 5 second at $500\mu N$ and a linear unloading rate of $100\mu N/s$). Figure 3.10 shows the result of such a quasi-static test on a single cell membrane in dry and wet condition (soaked for an hour). From Figure 3.10 it is observed that the segmental slope of the load-indentation depth curve for loading and unloading cycle is less for wet samples as compared to dry samples. It is also observed that creeping (increase of indentation depth at a constant frequency) is more for wet samples as compared to dry samples.

To understand the dynamics of wet and dry pads a ramping quasi-static test is done. The quasi-static load is increased linearly while the dynamic load is increased to a fixed

percent (10%) of quasi-static load at each step and the frequency applied is held constant (50Hz). Each point in Fig 3.11 is the material response to the maximum quasi-static load and it is clearly seen that the wet sample takes less load to penetrate into the sample as compared to dry sample. The segmental slope of load-indentation depth due to dynamic un-loading at a frequency of 50Hz at each step is shown in Fig. 3.12. The soaked pad shows lower contact stiffness K_s as compared to a dry pad. This trend can be further used to explain the non-uniformity in pressure distribution in the CMP process when the pad is in dry state or in soaked state due to abrasive slurry.

It is interesting to note that the reduction in stiffness is not that significant because the pad material is impermeable to water and most of the water penetrates only the topmost layer of voids in the material. Ng, et al. (2003) showed that the water absorption is limited to the outer layer of the pad surface and may alter its properties. From the experimental data [Ng et. al. 2003] it shown that the percentage volume of water-filled voids with respect to the pad volume is 3.4 percent, which is much lower than the 35 percent void volume of the pad. This means that only a fraction of the voids in the pad are filled with water. This is due to the impermeability of the pad and the fact that the voids are voids are closed cell, indicating little or no interconnection between voids. It is also observed from the pad weight (percent) versus soaking time (hrs) for IC 1000 pad that water takes very long time to penetrate the voids. This might be because of the fact that when the pad was first submerged under water, air gets trapped in the voids and some mechanism takes over until all the air pockets are filled with water.

3.5 Summary

- The dynamic (visco-elastic) properties of the dry IC 1000 pad are presented and the responses of dry and wet pad are compared in this work.
- An experimental measurement of the linear viscoelastic behavior of the surface of the pad in contact with a conical indenter is obtained.
- Variation of stiffness, damping coefficient, relaxation time with frequency and depth at constant frequency is obtained to using a simple mechanical Voigt model in the Dynamic Model for Nanoindenter system, which is in contact with specimen.

- The variation of contact stiffness, damping coefficient and reduced modulus with depth is due to the combination of local indentation and bending of the cell membrane of the porous pad.
- The variation of loss tangent as a function of frequency represents a plateau zone and the characteristic feature of the plateau zone is that the magnitude E'' is smaller than that of E'.
- Pad soaking tests indicate that the reduction of stiffness is not significant because the pad material is impermeable to water and most of the water penetrates only the topmost layer of voids in the material.

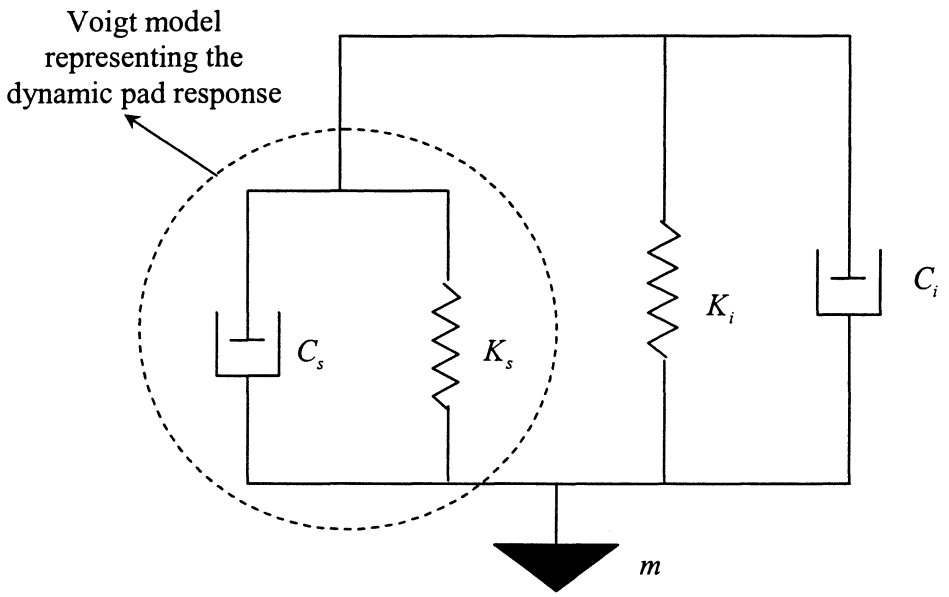

Figure 3.1: Dynamic model for Nanoindenter system including the effective dynamic pad response as a Voigt model

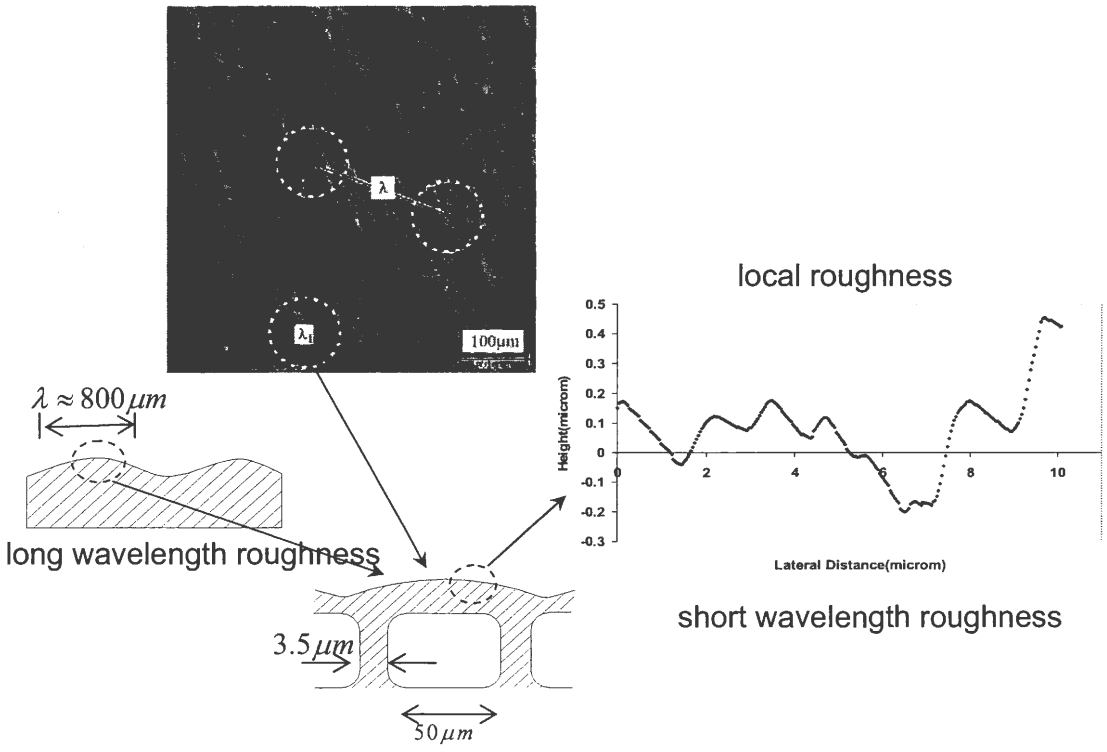

Figure 3.2: SEM image of a preconditioned pad surface morphology (IC1000) and pad morphology at different length scales

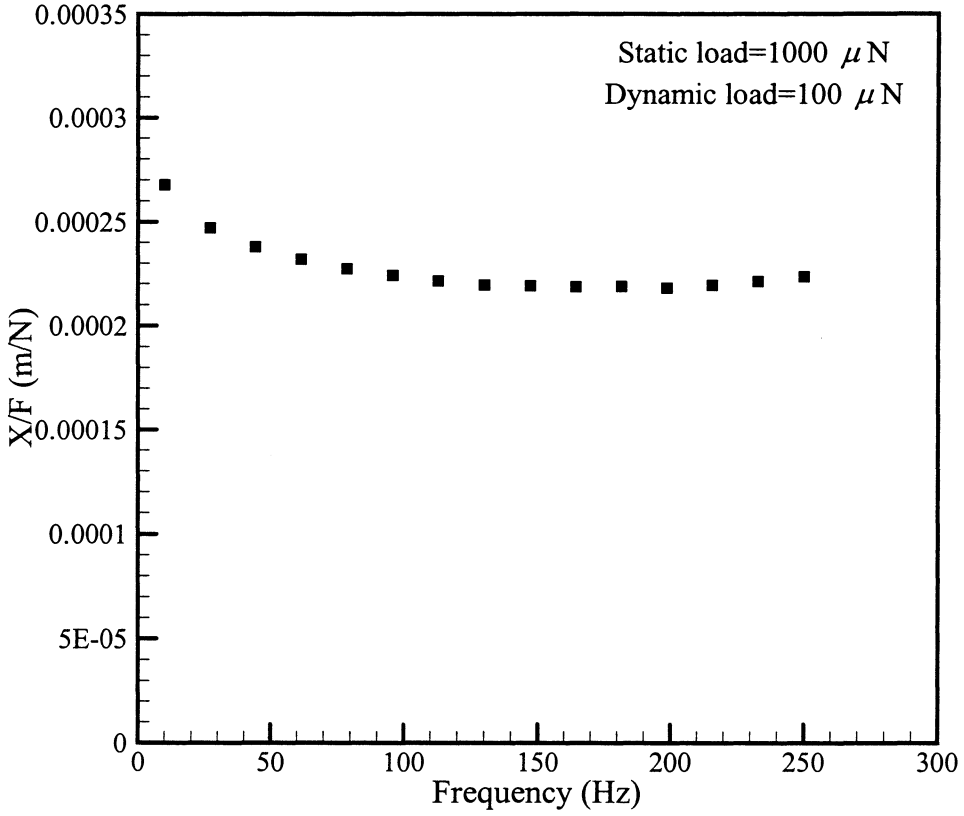

Figure 3.3: Plot for the ratio of harmonic displacement (X) over the amplitude of the harmonic force (F) as a function of frequency for a load of 1000micro Newton

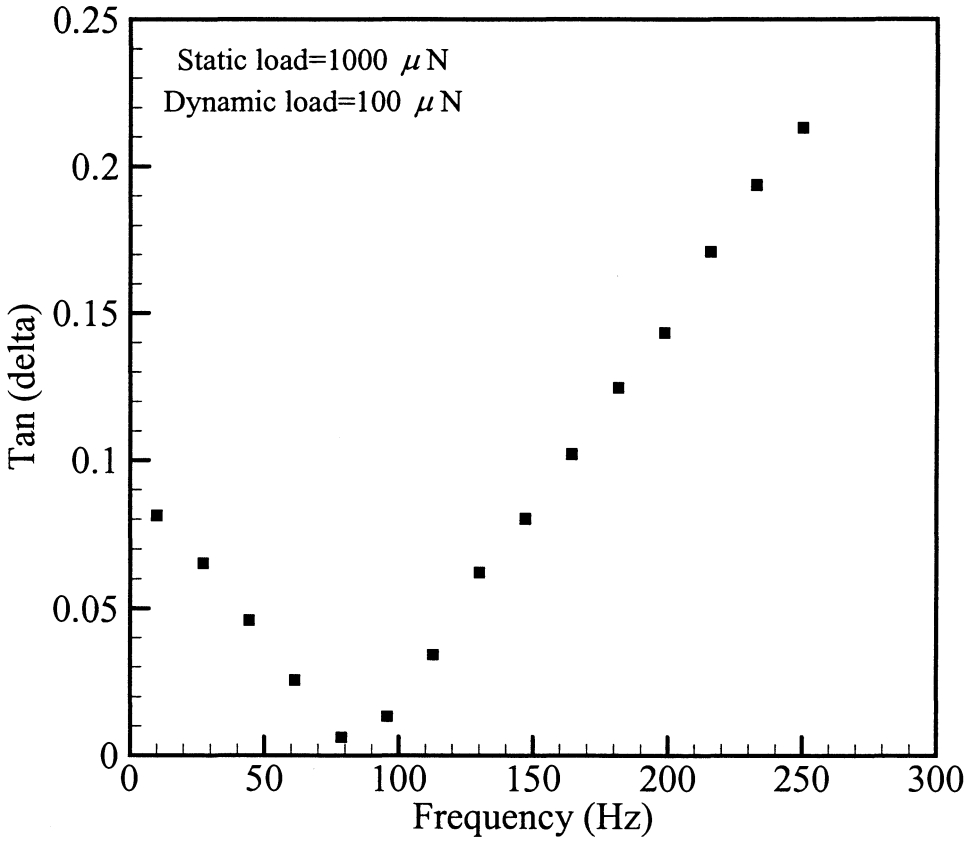

Figure 3.4: Evolution of Tan (delta) as a function of frequency at constant quasi-static and dynamic load

(a)

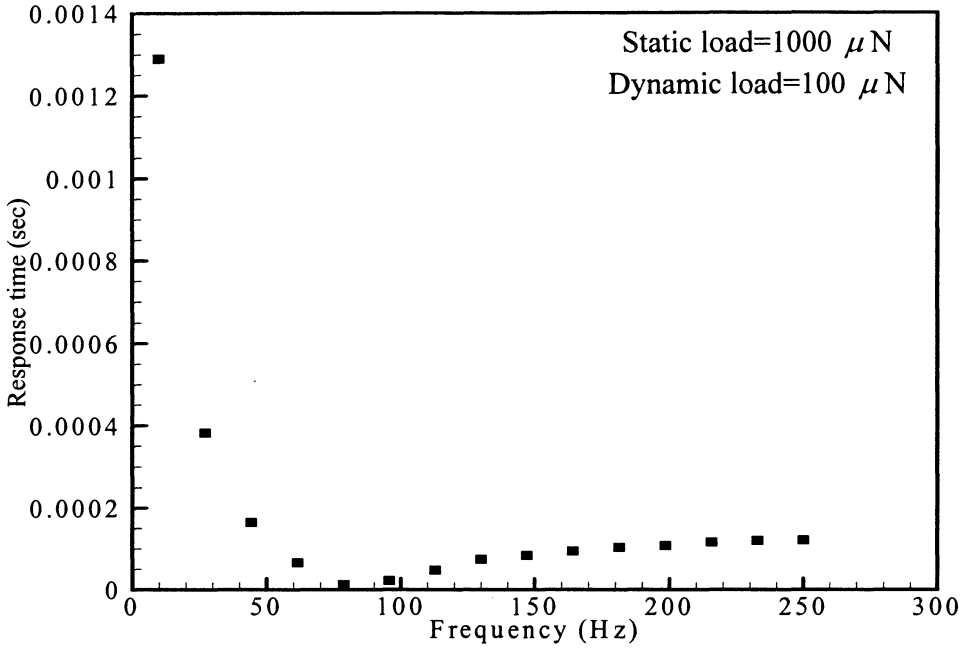

(b)

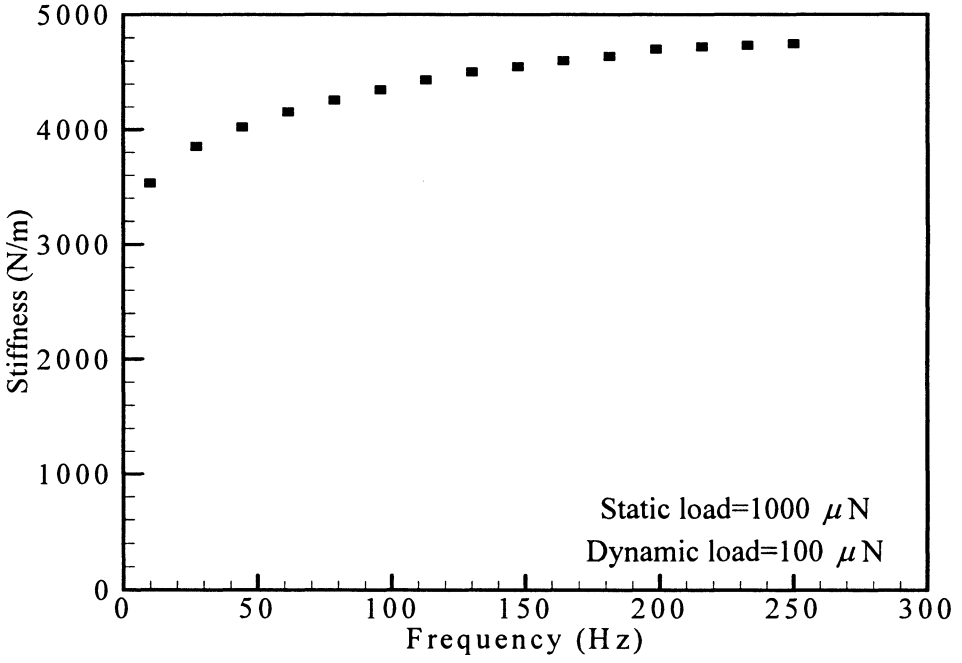

Figure 3.5: Voigt model analysis of (a) the response time τ and (b) stiffness K_s of the contact showing changes as a function of frequency

(a)

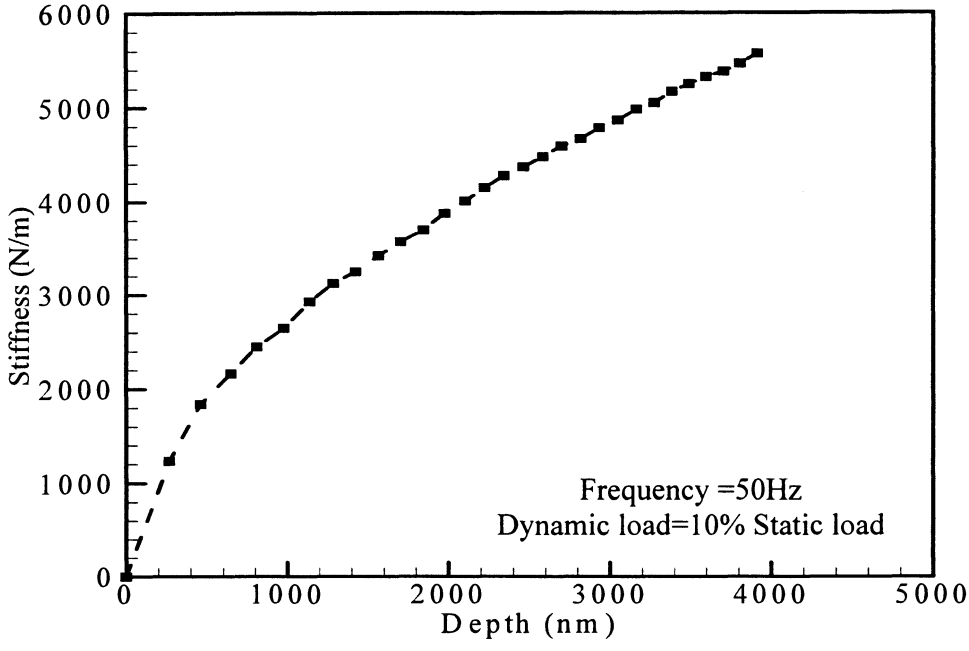

(b)

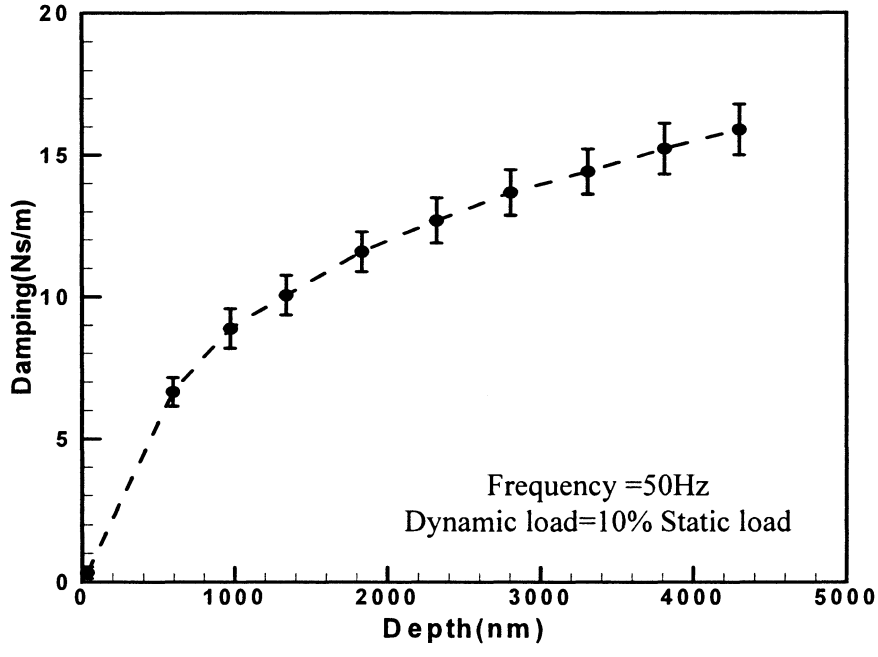

Figure 3.6: a) The contact stiffness variation as a function of depth of penetration b) the variation of damping coefficient as a function of depth of penetration

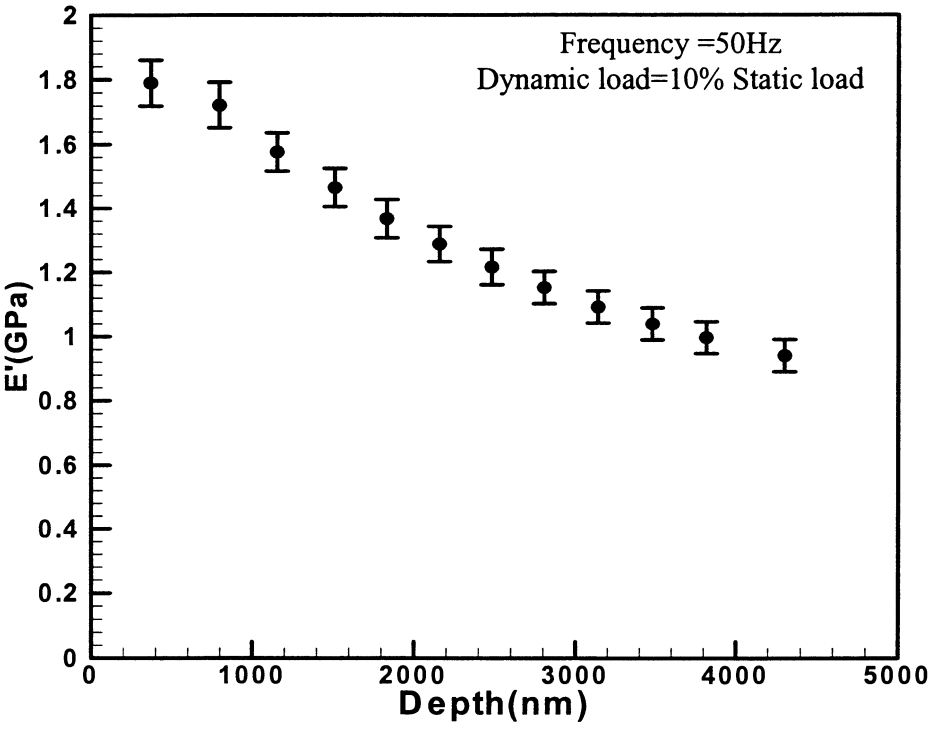

Figure 3.7: Variation of storage modulus E' with depth of indentation

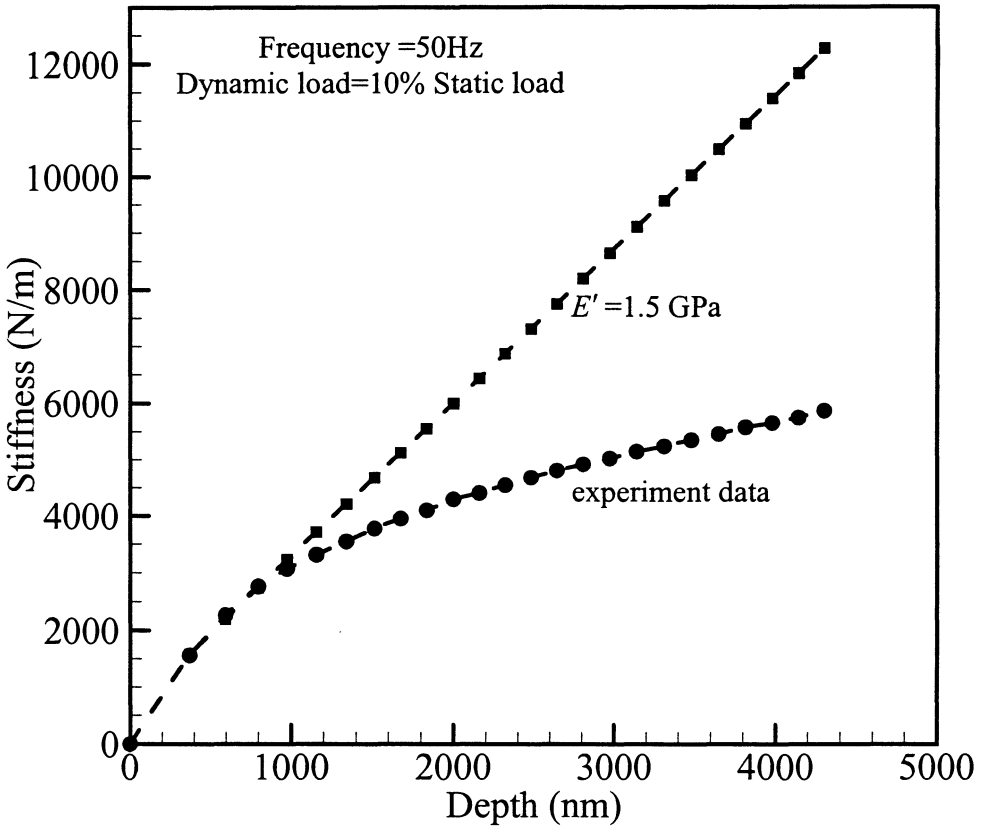

Figure 3.8: Contact stiffness comparisons of experimental data and the model (E'=1.5 GPa) with variation of depth

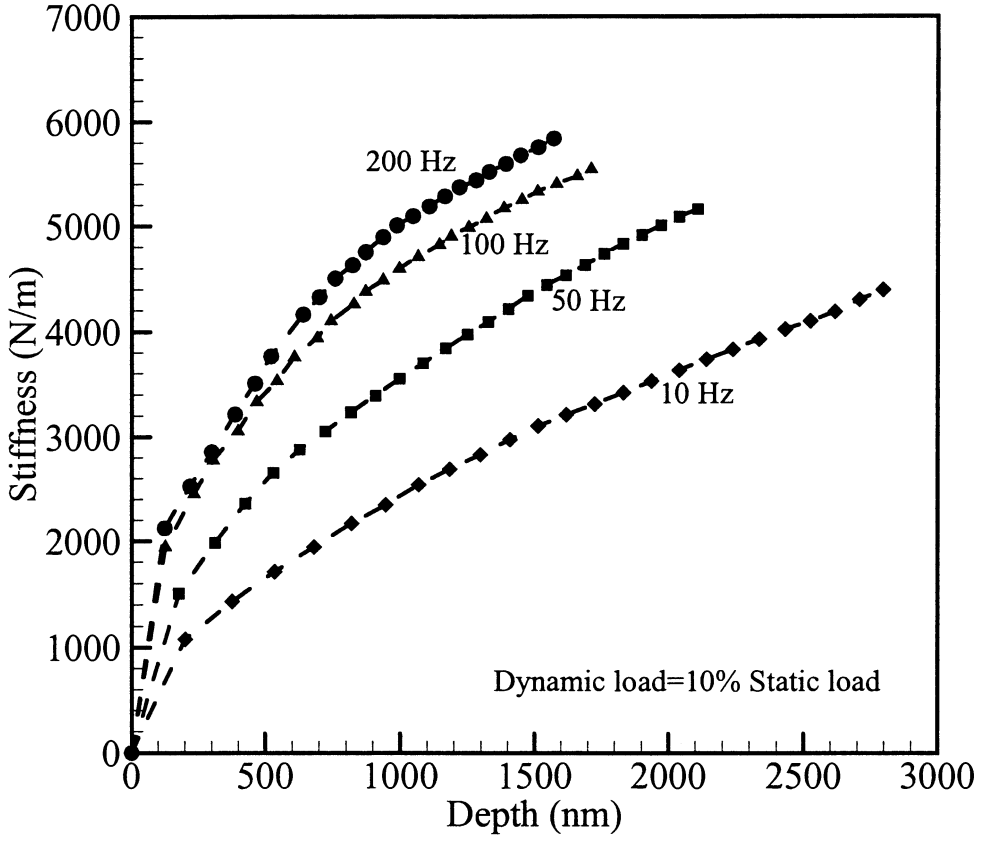

Figure 3.9: Variation of stiffness with depth at different frequencies

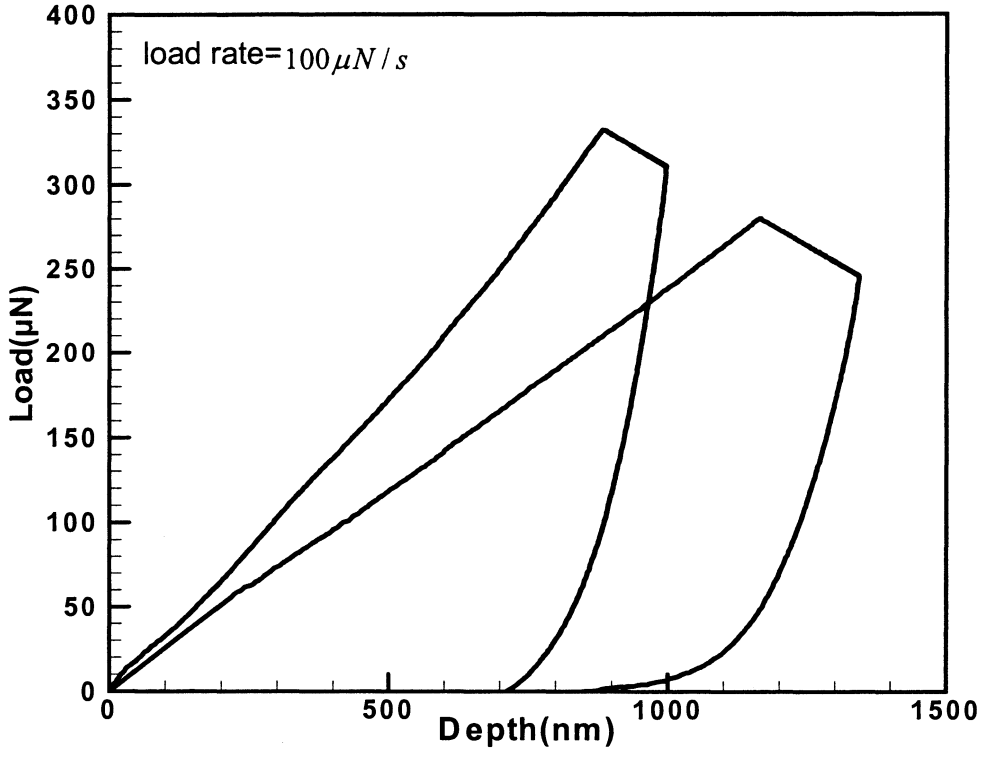

Figure 3.10: Comparison of loading and unloading cycle for dry and wet tests

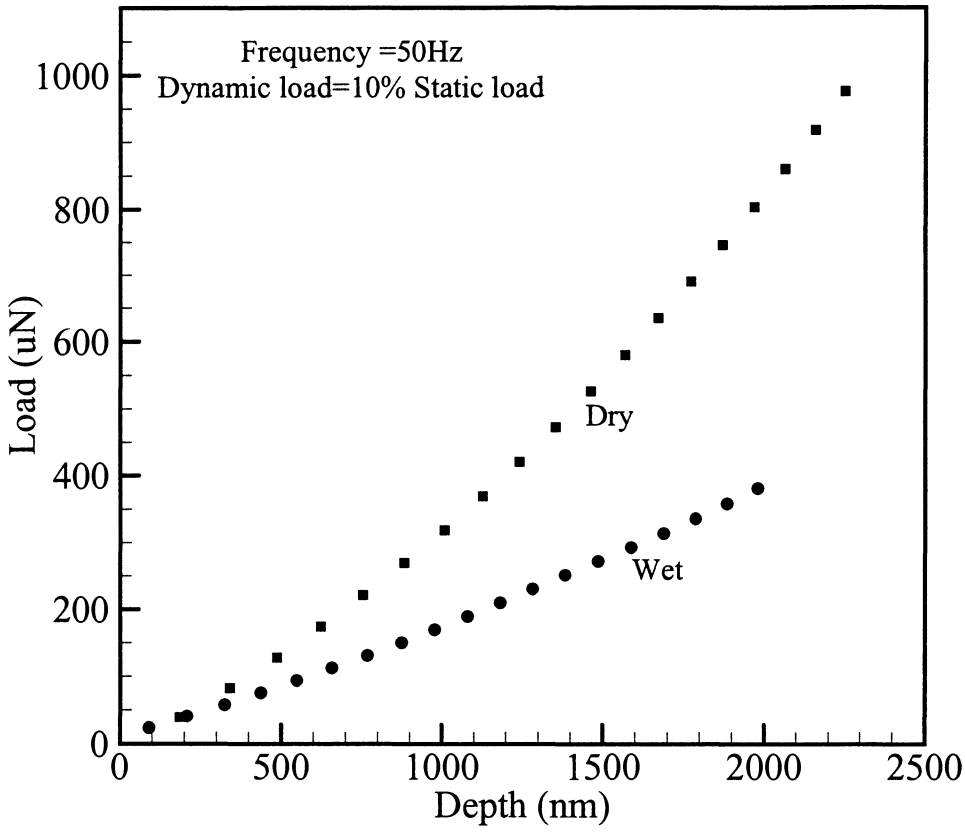

Figure 3.11: Comparison of Load vs Depth plots for dry and wet samples at a frequency of 50Hz and ramping quasi-static load

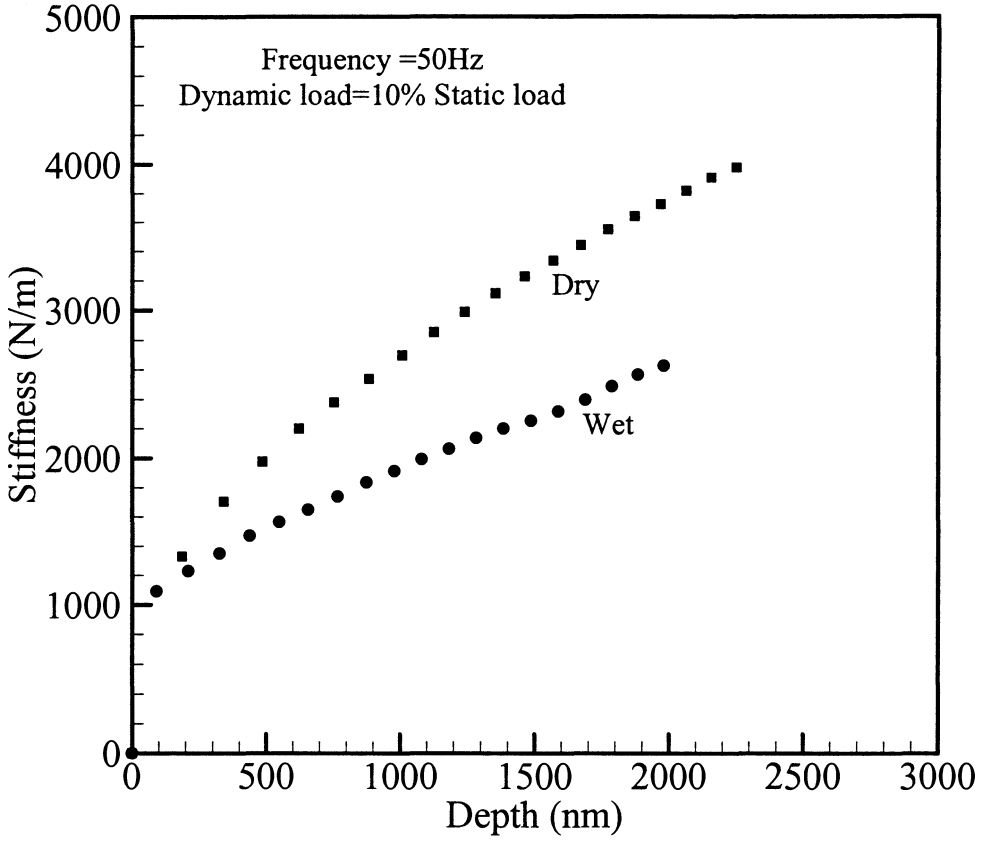

Figure 3.12: Comparison of stiffness v/s depth plot for dry and wet tests at a frequency of 50Hz and ramping quasi-static load

CHAPTER 4. CONCLUSIONS AND FUTURE WORK

4.1 Conclusion

Although the CMP process has existed for a long time, the materials aspects and mechanics aspects of the CMP pad is still poorly understood. There is also lack of integration of models at different scales in CMP. For example, feature scale, die scale and wafer scale models should be related to each other; but there is not much investigation about this. In Chemical Mechanical Polishing, there is lack of understanding about how the chemical part and the mechanical part interact. The purely chemical part is only wet etching and purely mechanical part is only dry polishing. In the mechanical part temperature rise during polishing, stiffness of the pad, size and distribution of the abrasive particles and pressure distribution are the factors which affect the CMP performance.

In this work the mechanics and the deformation mechanisms of the pad at micro and nano scale has been studied experimentally. The experimentally observed trends from quasi-static tests and deformation mechanisms indicate that the whole CMP process domain is carried out by local pad cell level interaction at the contact interface and not by the bulk response of the pad. It is found that the pad response is controlled by both the local indentation of the pad cells as well as the flexing deformation of the cell wall. The force-displacement plot obtained from the elastic response of the pad by quasi-static tests matches well with the series- spring mechanical model. The spherical Hertzian contact model is used along with cell bending model to form a series spring-mechanical model at shallow depth and the conical Hertzian contact model is used along with cell bending model to form a series spring-mechanical model at higher depth. It is also observed that cell bending is substantial as compared to local indentation at higher depths.

The dynamic (visco-elastic) properties of the dry IC 1000 pad are presented and the responses of dry and wet pad are compared in this work. An experimental measurement of the linear viscoelastic behavior of the surface of the pad in contact with a conical indenter is obtained. Variation of stiffness, damping coefficient, relaxation time with frequency and depth at constant frequency is obtained to using a simple mechanical Voigt model in the dynamic model for the Nanoindenter system, which is in contact with specimen. The

variation of contact stiffness, damping coefficient and reduced modulus with depth is due to the combination of local indentation and bending of the cell membrane of the porous pad. The variation of loss tangent as a function of frequency represents a plateau zone and the characteristic feature of the plateau zone is that the magnitude E'' is smaller than that of E'. Pad soaking tests indicate that the reduction of stiffness is not significant because the pad material is impermeable to water and most of the water penetrates only the topmost layer of voids in the material.

The implication of such findings is significant for enhancement of material removal rate while maintaining local and global planarization. This work can be further extended, in building a material removal model that incorporates the elastic and visco-elastic response of the pad at wafer scale, cell level and particle scale (Multi-Scale).

4.2 Future Work

In a CMP process the trend of polisher design is to use lower down force and higher velocity. The velocity may be high enough that viscoelastic pad deformation may significantly influence the CMP planarization efficiency. The present MRR model assumes elastic deformation by using a constant pad stiffness value. So the first step of future work is to build a mechanism-based material removal model, which incorporates visco-elastic effect of the pad, bulk response of the pad, local deformation and cell-bending phenomenon.

In this work a linear visco-elastic model (dynamic model) is used for the Nanoindenter system, which is in contact with specimen. In a real case the pad response is more complex and so a non-linear viscoelastic material model has to be developed as a second step of future work. This non-linear viscoelatic model should have four elements (two springs and two dashpots) that would represent a real pad material. The model predictions should then be compared with that of experimental trends. The according to the current literature the consistent pad topography after the first 5 minutes of polish does not correlate with the trend in the removal rate. The decay in the MRR occurred gradually over a period of 60 minutes. Hence, any decay in MRR between 5 and 60-minute time window cannot be attributed to the change in the surface topography of the pad. It is speculated that by

incorporation of non-linear viscoelastic pad properties would effectively capture the long-range decay of the MRR over the appropriate time scale.

The gained insights in pad deformation mechanism, viscoelastic properties and MRR model built for CMP process should be integrated into some kind of software package. This software package can be used to predict the MRR under different conditions, including complex surface topography, different operational parameters (like particle size and shape, particle concentration, down pressure and rotational speed) and different slurries.

Not much work has been done on addressing the issue of pad wear so the fourth step of future work is study pad wear and build a stochastic model for the effect of pad surface topography. In a CMP process, abrasive action combined with chemical attack causes pad asperities to wear, with high asperities wearing faster than low asperities. Such a study could give rise to longer pad life, better non-uniformity, improves slurry transport and lower defects.

REFERENCES

Bajaj, R., Desai, M., Jairath, R., Stell, M., and Tolles, R., 1994, "Effect of Polishing Pad Material Properties on Chemical Mechanical Polishing (CMP) processes," Material Research Society Symposium proceedings, Vol. 337, pp. 637-644.

Bastawros, A-F, Chandra, A., Guo, Y., Yan, B., 2002, "Pad Effect on Material Removal Rate in Chemical Mechanical Planarization", J. Electronic Materials, Vol.31 (10), pp. 1022-1031.

Boresi, A. P. and Sidebottom, O. M., 1985, "Advanced mechanics of materials", John Wiley & Sons, New York, pp.479.

Borucki, L., 2002, "Mathematical Modeling of Polishing Rate Decay in Chemical-Mechanical Polishing," J. Engr. Mathematics 43.

Doerner, M.F. and Nix, W.D., 1986,"A method for interpreting the data from depth-sensing indentation instruments", J. Mater. Res., Vol. 1, No. 4, pp. 601.

Ferry, J.D., 1980, "Viscoelastic Properties of Polymers", Wiley, New York.

Fu, G., Chandra, A., Guha, S., Subhash, G., 2001, "A Plasticity-Based Model of Material Removal in Chemical-Mechanical Polishing (CMP)". IEEE Transaction: Semiconductor Manufacturing, Vol. 14, No.4, pp. 406-4171.

Fu, G., Chandra, A., 2002, "A Model for Wafer Scale Variation of Material Removal Rate in Chemical Mechanical Polishing Based on Viscoelastic Pad Deformation", J. Electronic Materials, Vol.31 (10), pp. 1066-1073.

Gibson, L. J., Ashby, M. F., 1997, "Cellular solids structure and properties", 2nd ed., Cambridge University Press, Cambridge.

Gouda S. D., Bastawros A. F. and Chandra A., 2004a, "A Quantitative Analysis of Multi-Scale Response of CMP Pad: Quasi-Static Characterization of Dry Pad", J. Mater. Res., (Submitted).

Gouda S. D., Bastawros A. F. and Chandra A., 2004b, "A Quantitative Analysis of Multi-Scale Response of CMP Pad: Dynamic Characterization of Dry and Wet Pad" (in preparation).

Hsu J., Chiu S., Wang Y., Dai B., Tasi M., Feng M., Shih H., 2002, "The removal selectivity of titanium and aluminum in chemical mechanical planarization", J. Electrochem. Soc. 149 (3), pp. 204-208.

Izumitani, T., 1979, "Polishing, Lapping and Diamond Grinding of Optical Glasses," Treatise on Materials Science and Technology, Vol. 17, Academic Press, New York, U.S., pp. 115-172.

Johnson, K.L., 1999," Contact Mechanics", Cambridge University Press, Cambridge.

Kovalev, A., Shulha, H., Lemieux, M., Myshkin, N., Tsukruk, V.V., 2004, "Nanomechanical probing of layered nanoscale polymer films with atomic force microscopy", J. Mater. Res., Vol. 19 (No.3), pp. 716-728.

Loubet, J.L., Oliver, W.C., Lucas, B.N., 2000, "Measurement of the loss tangent of low-density polyethylene with a nanoindentation technique", J. Mater. Res., Vol. 15 (No.5), pp. 1195-1198.

Luo, J. and Dornfield, D.A., 2001, "Material removal mechanism in chemical-mechanical polishing: theory and modeling", IEEE Trans. Semicond. Manufact. 14 (2), 112-133.

Luo, J. and Dornfield, D.A., 2003, "Effect of Abrasive Size Distribution in Chemical Mechanical Planarization: Modeling and Verification", IEEE Trans. Semicond. Manufact. 16 (3), 469-476.

Martinez, M.A., 1994, "Chemical-Mechanical Polishing: route to global planarization," Solid State Technol., pp. 26-31.

Ng, S. H., Hight, R., Zhou, C., Yoon, I., Danyluk, S., 2003, "Pad Soaking Effect on Interfacial Fluid Pressure Measurements During CMP", ASME J. Tribol., Vol. 125, pp. 582-586.

Nguyen, V.H., Velden, P.V.D., Daamen, R., Kranenburg, H.V. and Woerlee, H., 2000, "Modeling of Dishing for Metal Chemical Mechanical Polishing," IEEE International Electronic Devices Meeting, pp. 499-501.

Oliver, W.C. and Pharr, G.M., 1992, " An Improved Technique for Determining Hardness and Elastic Modulus Using Load & Displacement Sensing Indentation Experiments", J. Mater. Res., Vol. 7 (No.6), pp. 1564-1583.

Pethica, J.B., and Oliver, W.C., 1987, "Tip Surface Interactions in STM and AFM", Physica Scripta. Vol. T19, pp. 61-66.

Runnels, S.R. and Eyman,L.M., 1994, "Tribology Analysis of Chemical Mechanical Polishing," J. Electrochem. Soc. Vol. 141 (No.6). pp. 1698-1701.

Shan, L., Levert, J. A., Meade, L., Tichy, J., Danyluk, S., 2000, "Interfacial fluid mechanics and pressure prediction in chemical mechanical polishing", J. Trib. 122 (3), pp. 539-543.

Sneddon I. N., 1965, "The Relation Between Load and Penetration in the Axisymmetric Boussinesq Problem for a Punch of Arbitrary Profile", Int. J. Eng. Sci. 3, 47.

Steigwald, M., 1997, "Chemical Mechanical Planarization of Microelectronic Materials," John Wiley & Sons. New York, pp. 66-84.

Syed Asif, S. A., and Pethica, J.B., 1998, "Nano-scale Viscoelastic Properties of Polymer Materials", Mat. Res. Soc. Symp. Proc. Vol. 505, pp. 103-108.

Ward, I. M., 1983, " Mechanical Properties of Solid Polymers," Wiley, New York.

Yu, T. K., Yu, C.C., and Orolowski, M., 1993, "A statistical polishing pad model for chemical-mechanical polishing, IEEE IEDM Washington DC, 865-868.

Zhou, C., Shan L., Hight R., Danyluk S., Ng S. H., and Paszkowski A. J., 2002, "Influence of Colloidal Abrasive Size on Material Removal Rate and Surface Finish in SiO_2 Chemical Mechanical Polishing", Lubrication Eng., August issue, p. 35.

ACKNOWLEDGMENT

First I would like to thank my major Professors Ashraf Bastawros and Abhijit Chandra, who have always given me all the support and cofindence. I really appreciate their their patience in guiding me over the past two years. I also like to thank Wei Che and Mike in our group, for helping in experiments.

This work is supported by U.S. National Science Foundation under Grants no. DMI-0084736 and DMI-0323069.